ISSN 1063-7729, Astronomy Reports, 2019, Vol. 63, No. 7, pp. 571–594. © Pleiades Publishing, Ltd., 2019.
Russian Text © The Author(s), 2019, published in Astronomicheskii Zhurnal, 2019, Vol. 96, No. 7, pp. 570–593.

Parameter Determination for the Eclipsing Long-Period Dwarf Nova EX Dra from Photometric Observations during Different Activity States of the System

T. S. Khruzina[1*], I. B. Voloshina[1], S. Qian[2], M. Wolf[3], and V. G. Metlov[1,4]**

[1] *Sternberg Astronomical Institute, Moscow State University, Moscow, 119234 Russia*
[2] *Yunnan Observatories, Chinese Academy of Sciences, Kunming, People's Republic of China*
[3] *Astronomical Institute, Charles University, CZ-180 00, Prague, Czech Republic*
[4] *Crimean Astronomical Station, Sternberg Astronomical Institute, Moscow State University, Nauchnyi, Russia*

Received January 10, 2019; revised February 9, 2019; accepted February 28, 2019

Abstract—The results of a long-term photometric observations of the cataclysmic variable EX Dra acquired between 2014 and 2016 at the Crimean Station of the Sternberg Astronomical Institute (24 nights, more than 10 500 measurements) are presented. The observations were performed using CCD photometers mounted on 50-cm and 60-cm telescopes in the visible and red, during both quiescence and the active state. For completeness, photometric observations obtained at the Ondrejov Observatory in 2010 in the V and R Johnson filters are also used in the analysis. The new observations of EX Dra are used to derive the orbital period of the system, which agrees well with earlier determinations. A combined model that takes into account the radiation fluxes from the gaseous stream and a hot spot on the lateral surface of the accretion disk is used to determine the parameters of the system components (white dwarf, red dwarf, accretion disk and hot spot, and gaseous stream). Variations of the parameters when the system changes from one activity state to the other are considered. Six light curves displaying unsatisfactory agreement between the observed and theoretical light curves can be successfully fitted using a version of the combined model that includes hot spots on the secondary's surface. This model is able to qualitatively reproduce a secondary minima in the light curves that exhibits shifts of this minimum from phase 0.5. The parameters of dark spots on the red-dwarf surface were determined. The data obtained indicate that the outbursts in the EX Dra system are related to instability of the matter outflow from the secondary.

DOI: 10.1134/S1063772919070035

1. INTRODUCTION

Dwarf novae are close binaries containing a late-type star (the secondary) that fills its Roche lobe completely. The outflowing matter accumulates in a disk and accretes onto the white-dwarf (WD) primary. Dwarf novae got their name due to their recurrent outbursts with amplitudes of $2–5^m$ on timescales from several days to several months. The outbursts are due either to instability of the matter outflow rate from the secondary (the Mass Transfer Instability Model, MTIM) or thermal instability of matter in the accretion disk (the Disk Instability Model, DIM), so that the disk mode is switched from low-viscosity to high-viscosity (see [1] and references therein). Detailed photometric observations of dwarf novae at early stages of their outbursts and their analysis in the framework of these models can make it possible to draw conclusions concerning possible origins of the outbursts. Unfortunately, it is fairly difficult to predict the onset of the next outburst: even if it is known, the outburst cycle period (P_b) is a mean value, the system's brightness rises very quickly (usually within hours), and the duration of the active state is short. It is necessary to monitor such objects continuously over fairly long times exceeding P_b, which is not always possible due to the dwarf nova's observing conditions.

2. BRIEF REVIEW OF DATA ON EX Dra

The variable star EX Dra (HS 1804+6753) was first discovered in the Hamburg Quasar Survey [2]. Subsequent observations of the system [3] demonstrated that EX Dra is a long-period dwarf nova with an outburst amplitude of $2–3^m$ and an orbital period

*E-mail: kts@sai.msu.ru
**E-mail: vib@sai.msu.ru

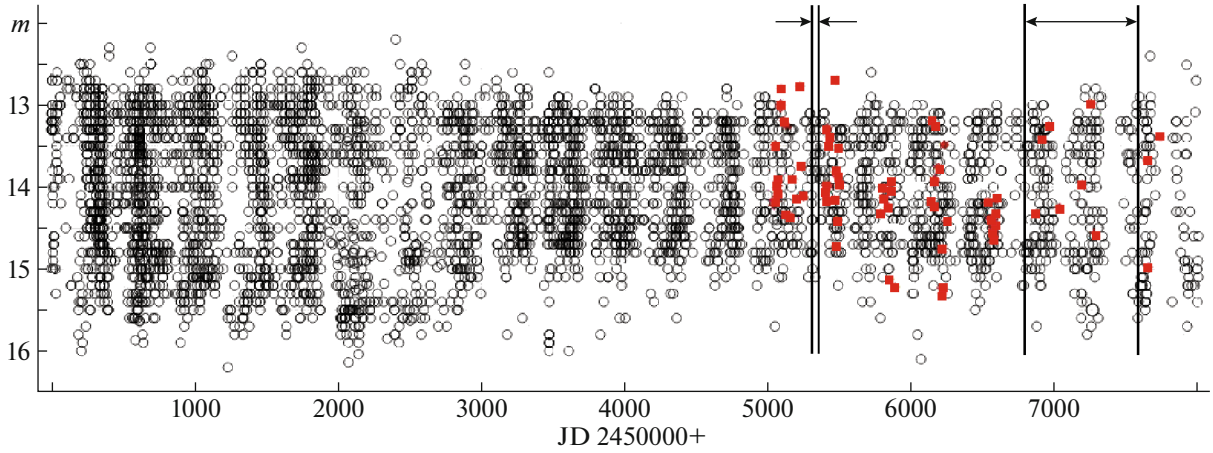

Fig. 1. Observations of EX Dra in white light (circles) and in the R filter (red squares) between 1995 and 2016 from AAVSO data. The vertical lines show the time interval of our observations used to determine the parameters of the system.

of $P_{orb} = 5.04^h$; i.e., the system is a long-period dwarf nova like EM Cyg ($P_{\rm orb} = 6.96^h$).

The light curves of EX Dra exhibit orbital variations with the ephemeris [4]

$$T_{\rm min} = {\rm HJD}\ 245\ 2474.80513(10) + 0.209\ 937\ 316(13)E + 18.4(9) \times 10^{-4} \sin\left(2\pi \frac{E - 3520}{36\,600}\right). \quad (1)$$

The numbers in brackets are uncertainties in the last digits of the parameter.

Spectroscopic studies of the system [5] indicate Hα emission lines in its spectrum formed near the hot spot on the accretion disk and/or near the inner Lagrange point L1. After correction for heating of the surface of the M1–2 V red dwarf (RD) with hot radiation from the WD primary, Billington et al. [5] obtained the semi-amplitude of the secondary $K_2 = 210 \pm 10$ km/s. Taking into account the radial-velocity curve of the WD, the component-mass ratio $q = M_1/M_2 \sim 1.25$ was found. The following basic parameters of EX Dra were derived in [6] based on an analysis of spectroscopic and photometric observations: $q = 1.34$, $i = 84.2°$, $M_1 = 0.75\ M_\odot$, $M_2 = 0.56\ M_\odot$. Baptista et al. [7] analyzed V and R light curves of EX Dra in quiescence and outburst and derived the following basic parameters from their analysis of eclipse profiles: $q = 1.39 \pm 0.12$, $i = 85° \pm 2.5°$, $M_1 = (0.75 \pm 0.15)\ M_\odot$, $M_2 = (0.54 \pm 0.10)\ M_\odot$, distance to the system $d = 290 \pm 80$ pc.

Shafter and Holland [8] present a study of $BVRI$ light curves of the system in quiescence (June 2–19, 2002) using a model taking into account four radiation sources: the primary (WD), the secondary (RD), the accretion disk, and the hot spot at the intersection of the gaseous stream with the outer edge of the disk. The width of the eclipse was used to put a lower limit on the orbital inclination, $i > 83°$ for $q > 1.23$. For the fixed temperature $T_2 = 3750 \pm 150$ K (corresponding to the RD spectral type M0–2 V), the best-fit temperature of the WD primary is $T_1 = 50\,000 \pm 20\,000$ K, the temperature of the hot spot is $T_s = 40\,000 \pm 10\,000$ K, temperature of matter at the disk's outer edge is $T_d = 6500 \pm 1000$ K, the disk radius is $R_d/\xi = 0.50 \pm 0.05$ (where ξ is the distance between L1 and the center of mass of the WD), and $\alpha_g = 0.3 \pm 0.2$ (where α_g is a parameter that depends on the viscosity of the matter in the disk, which determines the temperature change along the radius; $\alpha_g = 0.75$ for a stationary disk [9]). Using estimates of the secondary's absolute magnitude based on its spectral type ($8.8 < M_v < 9.7$), combined with the observed mid-eclipse brightness ($V = 16.57 \pm 0.05$) and extinction ($A_v = 0.45 \pm 0.63$), Shafter and Holland [8] determined the distance to EX Dra, $d = 240 \pm 90$ pc. A list of parameters of EX Dra found earlier in various studies is presented in Table 1.

Every 10–30 days, the EX Dra system undergoes outbursts that are up to 10 days in duration. Observations of the system from the AAVSO archive[1] in white light (circles) and in the R filter (red squares) for 1995–2016 are presented in Fig. 1. Two different states of the system, first discovered by Halevin and Henden [10], are clearly visible; according to their computations, the switch between the states occurred at JD 245 2665. Before this time, the system's brightness in quiescence (at minimum brightness) was $\sim 15.5^m$ (the out-of-eclipse flux during outbursts increased to 13.5^m); after this date, the brightness during eclipses increased to $\sim 15^m$ (the out-of-eclipse flux during outbursts decreased to $\sim 13^m$).

[1] The data were taken from the site www.aavso.org/LCGv2/

Table 1. Parameters of EX Dra from the literature

Parameter	Value	Reference	Parameter	Value	Reference
P_{orb}, days	0.20993718(2)	[8]		M0	[6]
	0.209937399(13)	[4]	Sp	M0 ± 2	[7]
	0.20993698	[7]		M1.5 ± 0.5V	[13]
i, deg	>83	[8]			
	85	[10]		163 ± 11	[7]
	85 ± 2.5	[7]	K_1, km/s	176	[12]
	84.2(6)	[6]		167	[5, 6]
	82.1	[12]			
$q = M_1/M_2$	1.34	[8]		224 ± 17	[7]
	1.39(11)	[7]	K_2, km/s	210	[5, 8, 12]
	1.25	[5]		223	[6]
	1.03–1.37	[12]			
M_1, $M_\odot$	0.75(15)	[6, 8, 10]		0.31(1)	[11]
	0.66	[5]	R_d, a_0	0.27(1)	[6]
	0.70	[12]	quiescence	0.267(4)	[7]
				0.21	[5]
M_2, $M_\odot$	0.56(2)	[6, 8]			
	0.54(1)	[7, 10]	R_d, ξ	0.50(1)	[7]
	0.52	[5]	quiescence	0.66	[11]
	0.59	[12]			
R_1	$0.013(1)R_\odot$	[6]		$0.471(2)a_0$	[6]
	$0.011(2)R_\odot$	[5, 7]	ξ	$0.85(4)\ R_\odot$	[6, 7]
	$0.0149a_0$	[7]		$0.82\ R_\odot$	[12]
	0.0317ξ	[7]			
R_2, $R_\odot$	0.57(4)	[6, 7]	R_d, a_0	0.49	[11]
	0.59	[12]	outburst		
T_1, K	28 000 ± 300	[7]	M_v	8.8–9.7	[8]
	50 000 ± 20 000	[8]	mag		
T_2, K	3850 ± 200	[7]	$E(B-V)$,	0.15	[7]
	3750 ± 150	[8]	mag/kpc		
a_0, $R_\odot$	1.63(2)	[6]		290 ± 80	[7]
	1.6(1)	[7]	d, pc	240 ± 90	[8]
	1.58	[12]			

A Fourier analysis of the outburst cycle shows [10] that, before the switch date, the mean outburst period was 23.9 days (varying smoothly between ∼18 and ∼30 days), while the outburst period decreased twofold after the switch, to 10–15 days. The outburst timescale became very unstable during this process.

Two approaches to explaining dwarf-nova outbursts are considered in [14], with the outbursts being due either to changes in the rate of mass transfer from the secondary (the MTIM model) or to thermal instability of matter in the accretion disk (the DIM model), so that a state with a low viscosity for the matter is replaced with a state with a high viscosity (see [1] and references therein). Observations of dwarf novae obtained in early stages of their outbursts can make it possible to explain the outburst as being associated with one of these models. The MTIM model predicts that the accretion disk should be compressed at the beginning of the outburst as a result of the abrupt increase in the outflow of matter with low angular momentum, while the brightness of the hot spot should increase in response to the higher matter ejection rate. Such effects are not expected in the DIM model. For example, recent observations of the intermediate polar EX Hya [15] indicate that the MTIM model is preferred as a description of the outbursts in this system.

We have studied optical light curves of EX Dra for March–April 2010 in the V and R filters and for May 2014–June 2016 in the Rc band. The aim of our study

was to test the hypothesis of Baptista [14] that the outbursts in this system are due to an increasing rate of mass outflow from the secondary rather than the thermal instability associated with changing viscosity in the disk.

Section 3 describes the observations of EX Dra and our determination of the binary's orbital period using observations during 2010–2016. The models of the close-binary system we used to determine the system parameters are briefly described in Section 4. Section 5 presents the results of our analysis, which are discussed in Section 6. The main conclusions of our study are summarized in Section 7.

3. OBSERVATIONS

We observed EX Dra in March–April 2010 at the Ondrejov Observatory (Czech Republic) using a 65-cm telescope and Johnson V and R filters. A G2-3200 CCD camera was used[2]. The exposure time in each filter was 90 s. The comparison star was GSC 04429–01414 ($V = 14.4^m$). Since its magnitudes in the visible and red were unknown at the time of our observations, the results are presented in relative units.

Observations of the system were obtained in 2014–2016 using CCD photometers mounted on the 50-cm and 60-cm telescopes of the Crimean Astronomical Station of the Sternberg Astronomical Institute. The detector used at the 50-cm telescope was an Apogee Alta U8300 CCD camera (3326×2504 pixels, 1 pixel $= 5.4$ μm), with the sensitivity maximum being 60% at 5800–6600 Å and 30% around 4000 Å. The detector used at the 60-cm telescope was an Apogee 47 CCD camera (1024×1024 pixels, 1 pixel $= 13$ μm). The length of the observing runs depended on the weather conditions and usually exceeded 5 h, in order to cover 1–1.5 orbital cycles. Our choice of the filter for the observations was based on the sensitivity of the light detector used, which was the highest in the red, Rc ($\lambda = 6700$ Å). The uncertainty of a single measurement was about the same for both telescopes, $\sigma \sim 0.02$–0.06^m. Since the object was faint, the exposure time varied from 40 to 60 s, depending on the weather. The details of our observations are presented in Table 2.

The main comparison star for our 2014–2016 observations was star No. 120 from the AAVSO list of standards, with coordinates $\alpha(2000) = 18^h03^m37.55^s$ and $\delta(2000) = 67^\circ57'01.7''$, in the immediate vicinity of EX Dra; this star has $B = 12.411^m$, $V = 12.038^m$, and $Rc = 11.832^m$. We verified the constance of the brightness of the standard star using several check stars. On three nights, we used star No. 134 as a comparison star. We also observed star No. 120 simultaneously on two of these nights, and so were able to compare the fluxes of EX Dra determined relative to the two comparison stars. On average, the difference was found to be $\Delta m = m(134) - m(120) = -0.002$ (some of the data points have the same fluxes in magnitudes), and the flux ratio to be $F(120) = 0.998\ F(134)$. For consistency, we reduced all our observations to the standard No. 120. We reduced our observations using the method of aperture photometry in the MAXIM-DL software package.

Seventeen of the 24 observational sets were obtained with the 50-cm telescope (2014–2015), and 7 series between September 2015 and June 2016 with the 60-cm telescope, while 2 series of Rc observations on one night (May 27, 2014) were obtained simultaneously on the two telescopes in order to determine any systematic difference between the measured fluxes. A comparison of the light curves shows that the Rc fluxes measured in the instrumental systems of the 50-cm telescope ($Rc(50)$) and the 60-cm telescope ($Rc(60)$) are related as

$$Rc(50) = Rc(60) + 0.05^m.$$

Here, $Rc(50)$ and $Rc(60)$ are expressed in magnitudes. Similar relations have been found for the cataclysmic variables GY Cnc [16] and ASAS-SN 13cx [17], which were also observed with these same telescopes. All further calculations were made for the light curves in the AZT-5 instrumental system.

Figure 2 shows the time distribution of our observations. The upper panel corresponds to the R observations (relative magnitudes),[3] and the lower panel to the Rc observations. The observations during outbursts, when the system's brightness increases by $\sim$1–1.2^m and the brightness at minimum increases by no more than $\sim$0.2–0.5^m, clearly stand out. The total amplitude of the light curves is $\sim 1.7^m$ in quiescence and $\sim 2.5^m$ during outburst.

All the Rc observations folded with the orbital period from Eq. (1) are shown in Fig. 3. Changes of the shape and amplitude of the light curves during outburst, compared to those during quiescence, are clearly visible.

The presence of a sine term in the orbital-motion ephemerides made it necessary to refine this term for

[2] See www.gxccd.com for details.

[3] We selected only complete light curves obtained on JD 245 5281–5316, which are to the left of the vertical dashed line; observations obtained at the Ondrejov Observatory after 2010 (to the right of the vertical line) cover only the region of the primary minimum, and were used only to determine the orbital period.

Table 2. Log of observations of EX Dra

Date, JD filter	T_1-T_2, date+	$\varphi_1-\varphi_2$	n	$T_{\min}$ (obs.)	$T_{\min}$ (theor.)	$m_{\min}$	$m_{\max}$
2455281, V	0.423–0.588	0.824–1.614	144	5281.45689	5281.45820	1.961	−0.179
2455294, R	0.424–0.655	0.752–1.854	210	5294.47576	5294.47714	1.668	−0.038
2455295, V	0.277–0.563	0.816–2.181	235	5295.52471	5295.52610	2.005	−0.133
2455309, R	0.347–0.622	0.835–2.148	250	5309.59021	5309.59139	1.318	−0.789
2455316, R	0.382–0.615	0.346–1.456	210	5316.51694	5316.51810	1.534	−0.085
2456790, Rc	0.284–0.497	0.019–1.032	266	6790.487916	6790.48864	15.089	13.003
2456805, Rc	0.291–0.494	0.503–1.472	344	6805.394538	6805.39514	15.524	13.428
2456806, Rc	0.278–0.480	0.205–1.168	252	6806.444571	6806.44508	15.370	12.935
2456819, Rc	0.376–0.498	0.596–1.177	147	6819.462557	6819.46396	15.525	13.925
2456834, Rc	0.281–0.497	0.592–1.619	378	6834.365058	6834.36635	15.528	14.130
2456916, Rc	0.300–0.508	0.277–1.264	706	6916.450335	6916.45050	15.411	13.314
2456960, Rc	0.195–0.550	0.359–2.053	1252	6960.327314	6960.32940	15.573	14.094
2457089, Rc	0.199–0.474	0.848–2.159	475	7089.439954	7089.44041	15.287	13.025
2457090, Rc	0.204–0.538	0.635–2.227	660	7090.280370	7090.28118	15.328	13.059
2457091, Rc	0.218–0.578	0.465–2.184	703	7091.329479	7091.33029	15.444	13.236
2457106, Rc	0.225–0.484	0.949–2.183	511	7106.236423	7106.23672	15.580	14.114
2457108, Rc	0.256–0.522	0.625–1.893	519	7108.337453	7108.33865	15.611	14.302
2457118, Rc	0.258–0.463	0.265–1.243	401	7118.411180	7118.41122	15.607	14.200
2457123, Rc	0.245–0.502	0.023–1.247	505	7123.451527	7123.45230	15.614	14.286
2457124, Rc	0.276–0.508	0.932–2.036	453	7124.290578	7124.29130	15.595	13.919
2457167, Rc	0.307–0.532	0.901–1.978	443	7167.330393	7167.33139	15.591	14.193
2457182, Rc	0.360–0.520	0.608–1.370	315	7182.441782	7182.441783	15.591	14.309
2457267, Rc	0.249–0.500	0.959–2.159	497	7267.257557	7267.25841	15.601	14.275
2457268, Rc	0.251–0.500	0.733–1.919	487	7268.308530	7268.30939	15.635	14.438
2457271, Rc	0.224–0.469	0.894–2.061	487	7271.245937	7271.24788	15.642	14.549
2457456, Rc	0.198–0.483	0.987–2.345	560	7456.200439	7456.20052	15.211	12.744
2457457, Rc	0.244–0.503	0.968–2.203	347	7457.250034	7457.25049	15.311	12.911
2457463, Rc	0.309–0.573	0.856–2.115	343	7463.335462	7463.33657	15.687	14.440
2457551, Rc	0.271–0.543	0.848–2.143	518	7551.302396	7551.30305	15.672	14.363

The second column gives fractions of the Julian day for the beginning and end of the observations for the corresponding date, and the third column the corresponding phase interval. For observations in 2010 (five dates), the two last columns present $m_{\min}$ and $m_{\max}$ relative to the comparison star.

the epoch of our observations. We performed this procedure separately for the R and Rc observations using the Lafler–Kinman method. Figure 4 displays the power spectra derived for the two sets of observations: the upper panel shows the spectrum for the R and lower panel those for the Rc observations.

We searched for the orbital period in the frequency range 4.7–4.8 days^{-1}, with a phase increment of 0.005. Bearing in mind the large time gaps between the individual groups of R observations, we searched for the orbital period using all the available data, as

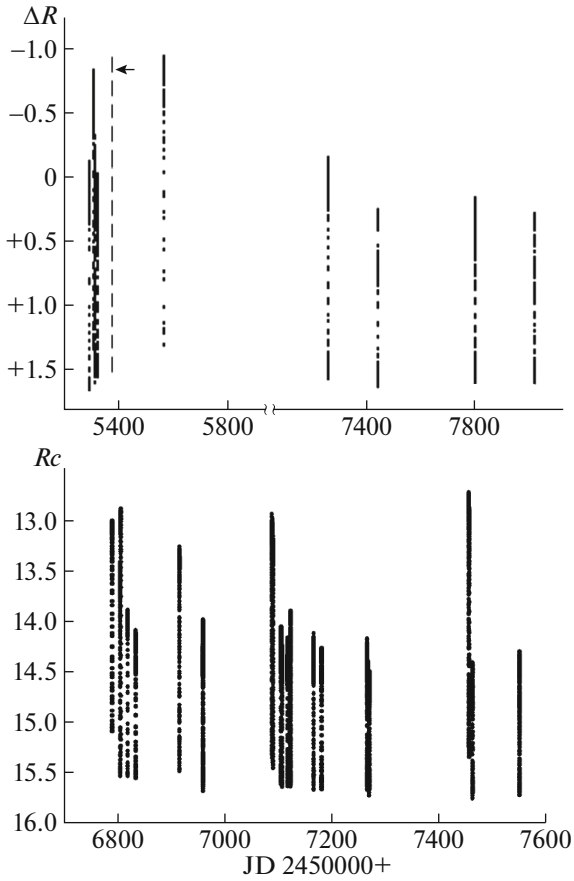

Fig. 2. Time distribution of the observations. The upper plot shows the relative R observations and the lower plot the observations in the Rc filter. The observations to the right of the dashed vertical line in the upper panel were used only to determination the system's orbital period, since they cover only phases near the primary minimum.

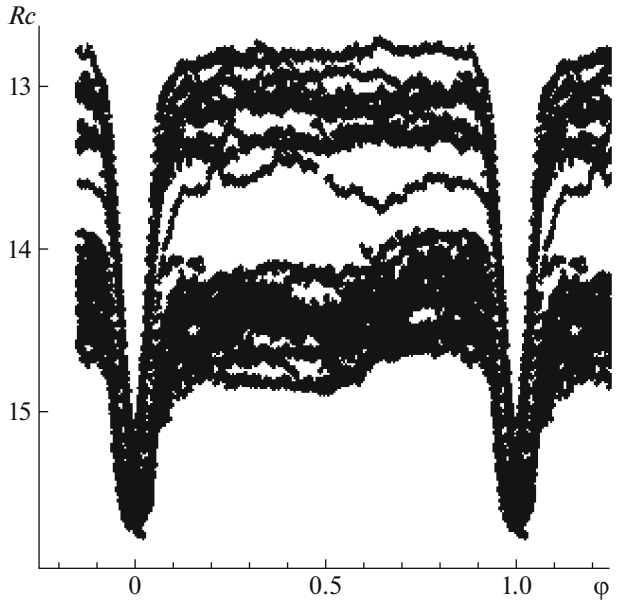

Fig. 3. All the Rc observations folded with the ephemeris (1).

well as individual fragments. The results of our analysis are the following.

(1) The period found for the wide range JD 245 5294–8014, $P_{\rm orb} = 0.209\,9374(5)^d$, coincides with the linear term of Eq. (1), $P_{\rm orb} = 0.209\,937\,399(13)^d$, taken from [4].

(2) The period found for the narrower range JD 245 5294–5567 is $P_{\rm orb} = 0.209\,9429(1030)^d$.

(3) The period found for JD 245 5294–5325 is $P_{\rm orb} = 0.209\,9576(1080)^d$. The significance of the formal period increase is reduced due to the increased uncertainty.

The period derived from our Rc observations (Fig. 4b) is $P_{\rm orb} = 0.209\,9366(6)^d$. Thus, all the derived periods coincide, within their errors, with the period determined in [4]; we used the latter, more accurate, period when folding the EX Dra light curves.

4. MODELS USED TO FIT THE OBSERVATIONS. DESCRIPTION OF INPUT PARAMETERS

As a whole, the shapes of the light curves of EX Dra in quiescence and during outburst are typical of dwarf novae (see Figs. 5, 6). Such curves can be successfully reproduced in the standard "combined" model, taking into account the presence of a hot line near the lateral surface of the accretion disk and a hot spot on the disk, on the leeward side of the gaseous stream [10].

A consideration of the light curves (JD 6805, 6834, 7167, 7267, 7271)[4] shows that the secondary minimum, though symmetric, is displaced to the orbital phase $\varphi \sim 0.6$ (this is especially obvious for the light curve for JD 7167); the out-of-eclipse part of the light curve for JD 6834 even shows two local minima (see Fig. 6a). Such displacements cannot be described in the standard combined model, since the hot spot is screened by the disk edge at these phases, and the gaseous stream is not visible at phases $\varphi \sim 0.5$ for $i > 83°$. The observed shift of the secondary minimum, and also the dips of varying depth in the light curves, can be reproduced if the contribution of the light from the secondary to the total flux is asymmetric. This effect can be created by the presence of one or two cool spots on the stellar

[4] Here and below, light curves obtained for a given Julian date, such as JD 245 6834, are labeled JD 6834, for brevity. The 2010 observations covered only 35 days, and we accordingly used even shorter abbreviations, for example, JD 295 for the date JD 245 5295.

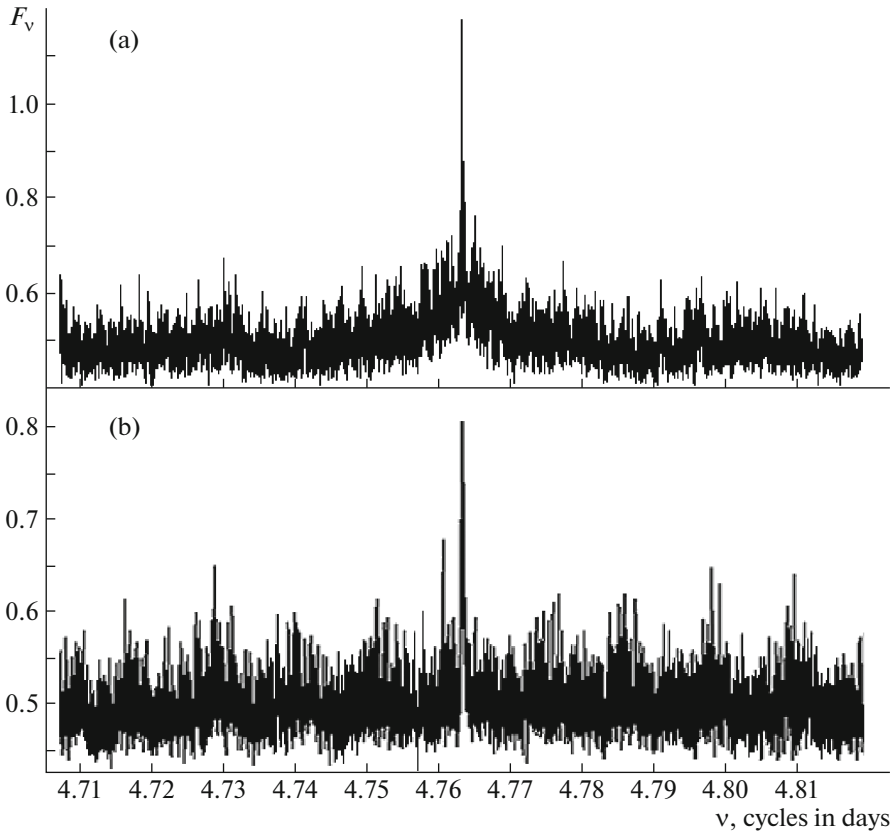

Fig. 4. The Lafler–Kinman power spectra constructed using the R (a) and Rc (b) observations.

surface. We used the software described in [19, 20] to take into account the presence of dark spots on the RD surface.

4.1. Main Features of the Combined Model

The system consists of a spherical star (primary), surrounded by an accretion disk, and a RD (secondary) that completely fills its Roche lobe. The star was divided into 648 area elements that emit radiation in accordance with their individual temperatures T_i, which depend on the secondary's effective temperature T_2. When computing T_i, we took into account the heating of the RD surface by radiation from the inner regions of the accretion disk with temperature T_{in}, $T_{in} \geq T_1$, where T_1 is the effective temperature of the primary. The shape and size of the secondary are determined by the parameter $q = M_1/M_2$. When computing the flux from an area element on the RD surface, we took into account gravitational darkening and limb darkening in a linear approximation.

The gravitational darkening is given by the formula $T_i = T_2(g/g_0)^\beta$, where T_i is the local temperature, g the local gravitational acceleration at the center of the area element on the surface of the tidally distorted, late-type star, and $\beta = 0.08$ [21]. The brightness of an area element on the star was described by the law $dI = B_\lambda(T)(1 - u(\lambda, T)(1 - \cos\gamma))\cos\gamma dS$, where γ is the angle between the normal to the area element on the stellar surface and the line of sight, $u(\lambda, T)$ the linear limb-darkening coefficient, $B_\lambda(T)$ the Planck function, and dS the area of the area element under consideration.

The primary was taken to be a sphere with radius R_1 located at the focus of a slightly elliptical accretion disk with eccentricity $e \leq 0.25$, semi-major axis a, and position angle α_e (taken to be the angular distance in the orbital plane between the disk periastron and the line connecting the centers of mass of the components). The disk was taken to be optically thick and to have a complex shape, being geometrically thin near the surface of the WD and geometrically thick at its outer edge, with an opening angle β_d. The temperature of each area element on the disk is given by $T(r) = T_{in}(R_{in}/r)^{\alpha_g}$, where R_{in} is the radius of the first orbit near the primary, $R_{in} \sim R_1$, and α_g depends on the viscosity of the gas in the disk, α_H. In the stationary case, $\alpha_g = 0.75$ [9]; when α_g decreases, the flux from the disk increases considerably due to the shallower radial distribution of the disk temperature. When computing the local temperature of a selected area element on the disk, we took into account heating by radiation from the secondary (this

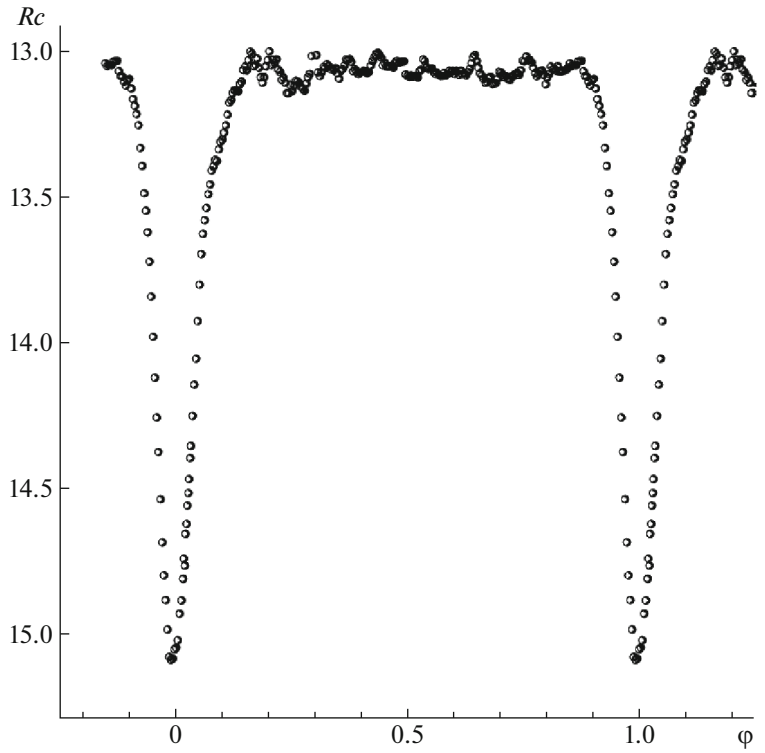

Fig. 5. Typical appearance of the light curves of EX Dra during outburst. Unaveraged observations (JD 6790) are plotted.

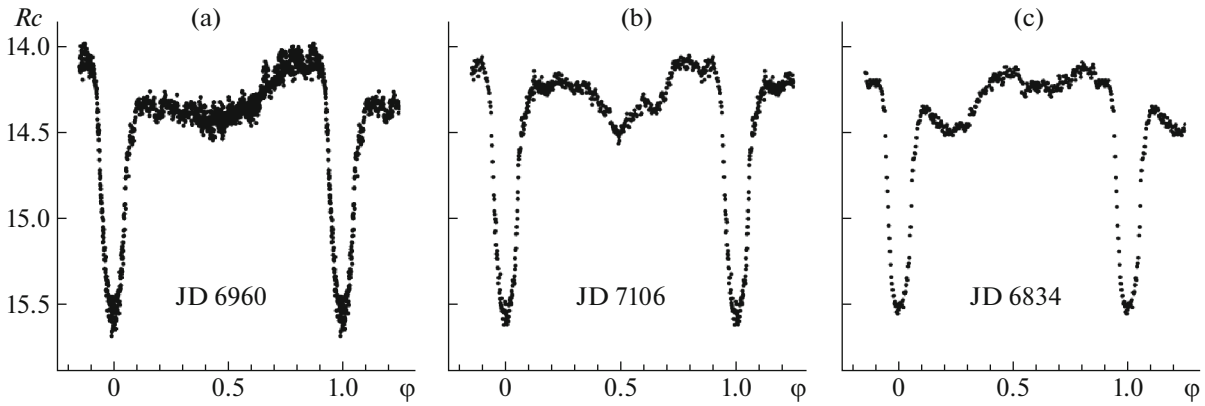

Fig. 6. Typical light curves of EX Dra in quiescence.

effect is usually insignificant), as well as heating by high-temperature radiation arriving from the inner parts of the disk.

The other emitting components are the following (see the detailed description in [18]).

1. The region where the gaseous stream collides with the disk, located near the disk surface. The interaction between the stream and the disk is shockless; a shock appears in a narrow region near the edge of the stream (the "hot line", HL) as a result of the interaction between the incoming flows from the disk and near-disk halo and the matter of the stream. The emitting region of the HL is described with a truncated ellipsoid whose center is in the orbital plane, inside the body of the disk. In the model we used, the region of energy release consists of two regions on the surface of the truncated ellipsoid (parts of the HL ellipsoid outside the body of the disk), on its windward ($\varphi \sim 0.25$) and leeward ($\varphi \sim 0.75$) sides.

2. The hot spot (HS) on the lateral surface of the disk, on the leeward side of the stream. Here, the emitting region is represented with a half ellipse whose center U coincides with the point where the axis of the gaseous stream intersects the disk.

Our final tables present the following parameters

of the regions of interaction between the gaseous stream and the lateral surface of the disk determined in our analysis: the semi-axes a_v, b_v, c_v of the ellipsoid whose part outside the body of the disk describes the shape of the gaseous stream; the maximum temperatures of the matter in the stream at the boundary with the disk, to the windward, $T_{ww,\max}$, and leeward, $T_{lw,\max}$, sides of the ellipsoid (with increasing distance from the disk edge, the temperature of the matter in the HL decreases according to a cosine law); the angle β_1 between the axis of the gaseous stream and the line joining the binary components (calculated in the process of the computations); the radius of the HS on the lateral surface of the disk R_{sp}, which is the distance between the point U and the outer edge of the spot in the orbital plane. Part of the HS is inside the gaseous stream; i.e., the actual size of the HS on the disk surface is smaller, but the radiation from the "obscured" part of the spot is compensated by the emitting regions on the leeward side of the stream. All the geometric parameters are expressed in the units of the distance between the component centers of mass a_0 (the software assumes $a_0 = 1$).

4.2. Main Features of the Model with Spots on the Secondary's Surface

This model (which we will call the "spot" model) is based on the combined model described above, with the addition of one or two "dark" spots on the surface of the RD.[5] The effective temperature of the area elements in the regions of these spots are lower than the temperature the area would have in the absence of the spot by a factor F_s; i.e., $T(x_s, y_s, z_s) = F_s T_2(x, y, z)$. The parameter F_s was assumed to be constant within a spot. Projected onto a plane tangential to the stellar surface at the point (x_s, y_s, z_s), the spots are circular with radius R_s, expressed in units of the stellar radius r_i at the point under consideration. We specified the position of the spot center on the surface using the two angles η and ϕ, where η is the spot's latitude measured from the tip of the star's "nose" towards the back hemisphere ($0° < \eta < 180°$) and ϕ is its longitude ($0° < \phi < 360°$) measured clockwise from the orbital plane; the zero meridian lies in the orbital plane, in the star's left hemisphere as viewed from the primary. The condition for an area element on the star's surface with the central coordinates (x, y, z) or (r, η, ϕ) to be found in the region of a spot is $(x - x_s)^2 + (y - y_s)^2 + (z - z_s)^2 < R_s^2$.

[5] In principle, there can be any number of spots; however, four independent parameters (R_s, F_s, η, ϕ) are needed to describe each of the spots, and the search for the best-fit parameters becomes much more difficult, even in the case of two spots.

The number of unknown parameters in a model with two dark spots increases by eight, with these additional parameters being directly related to the dark spots. Thus, it is reasonable to use this model when the main parameters (those of the disk, HL, HS) are fixed or vary in sufficiently narrow ranges.

We solved for the parameters in both models yielding a synthetic light curve shape that was maximally close to the observed light curve using the Nelder–Mead method [22]. When searching for the global minimum of the residuals for each of the light curves, we used several dozen different initial approximations, with several local minima usually present in the studied parameter domain for a large number of independent variables. To estimate the degree of agreement between the theoretical and observed light curves of the close binary in the model used, we calculated the χ^2 residuals in the form

$$\chi^2 = \sum_{j=1}^{J} \frac{(m_j^{\text{theor}} - m_j^{\text{obs}})^2}{\sigma_j^2},$$

where m_j^{theor} and m_j^{obs} are the magnitudes of the object at orbital phase j derived theoretically and from the observations, σ_j is the dispersion of the observations for point j, and J is the number of normal points in the mean light curve.

5. MODELING RESULTS

Since the number of imput parameters is fairly large (q, i, T_1, T_2, R_1, R_d, A,[6] α_e, $e < 0.25$, α_g, a_v, b_v, c_v, $T_{ww,\max}$, $T_{lw,\max}$, R_{sp}), we limited the region of their possible values taking into account data obtained earlier from spectroscopic and photometric observations (see Table 1).

We computed the parameters of the synthetic curves used to describe the observations in two stages. In the first, the most "classical" light curves were used to determine the basic parameters of the system (q, i, T_1, T_2, R_1). Since the light curves we obtained form a sequence of uniform data (the observations were reduced to the same instrumental system, and the same comparison star was used), we can impose an additional restriction on the region of permitted parameters of the problem. Namely, when several light curves were present, we translated the synthetic light curves into magnitudes using a uniform energy unit: the flux from the system $F(m)$ corresponding to the same magnitude m for all the

[6] A is the parameter of the paraboloid that describes the inner (not lateral) surface of the disk; usually $A \sim 6$–12. The lower the value of A, the greater the thickness of the disk's outer edge β_d.

light curves we used for the corresponding filter. In this case, it is possible to compare the synthetic and observed light curves based not only on their shapes, but also on changes in the level of the radiation flux. A detailed description of this technique can be found in many of our earlier studies (e.g., [23], as well as the recent publications [16, 17]).

As a result of the first stage of our analysis, we selected the following basic parameters: $q = 1.34$, $i = 83.5°$, $R_1 = 0.0315\xi = 0.0167a_0$. The mean radius of the secondary is determined by the component-mass ratio and, for $q = 1.34$, is $\langle R_2\rangle = 0.3649a_0$; $\xi = 0.5301a_0$. We did not fix the temperatures of the stars, but limited their range to the range for M0±2 V stars (3400–3700 K [24]) for the secondary and to the interval 19 000–35 000 K for the primary, due to the considerable variations of the T_1 values found for different light curves in the first stage of our computations. For the energy units, we adopted $F(Rc = 13.5) = 0.1658 \times 10^{-9}$, $F(\Delta R = 0.0) = 0.11477 \times 10^{-9}$, and $F(\Delta V = 0.0) = 0.11056 \times 10^{-9}$ relative units. Our use of relative units is due to the fact that the Planck function used to compute the fluxes from the system components per unit wavelength interval (in our case, in centimeters) is the energy flux passing through a 1 cm^2, area, while the unit of distance in the code was a_0, the distance between the close-binary components, so that $a_0 = 1$ and its value in physical units (e.g., cm) is not known beforehand.

In the second stage, we searched for the best-fit parameters of the system. Tables 3–5 present the parameters of the components derived using the three R, two V, and 18 Rc light curves in the combined model, in both quiescence and outburst. Table 6 presents the parameters for six light curves (JD 6805, 6834, 7108, 7167, 7267, 7271) computed with the spot model, since the shapes of their out-of-eclipse parts could not be adequately fitted with the combined model. The lower parts of each of these tables contain the contributions of various components to the combined flux, averaged over the orbital period. We estimated the parameter uncertainties by specifying a conditional boundary inthe residual of $1.1\chi^2_{\min}$ for a selected light curve. This estimate does not yield the canonical uncertainty of the corresponding parameter based on a χ^2 criterion, but enables us to estimate its stability with respect to variations. The uncertainties in the last digit of each parameter estimated in this way are given in parantheses.

Figures 7, 8 show the unaveraged observed R and V light curves of EX Dra and the light curves synthesized using the parameters from the corresponding tables. Figures 9–11 display the Rc light curves in quiescence, Figs. 12 and 13 the Rc light curves during outburst, and Figs. 14 and 15 the Rc light curves synthesized using the parameters from Table 6 obtained with the spot model. To the bottom or to the right, we present the contributions from the system components to the combined light for each date in relative units.

5.1. V Light Curves. Quiescence

Our analysis of the V data demonstrates (Fig. 7, Table 3) that both light curves were obtained in quiescence. The total variation amplitude did not change with time; the depth of the secondary minimum decreased slightly, and the amplitude of the flux fluctuations also decreased. Comparing the parameters derived for the JD 281 and JD 295 light curves, we find that the disk radius increased from 0.4ξ to 0.5ξ, and the thickness of the disk's outer edge decreased by almost a factor of two. The steeper radial temperature distribution in the disk, due to an increase in α_g by a factor of 1.3, has the result that the temperature at the disk's outer edge became lower by ∼1700 K, despite the higher temperature T_{in} in the boundary layer (by almost 3000 K). Formally, the period-averaged contribution of the disk to the total flux, F_d/F_{full}, remained the same within the uncertainties. The azimuth of the stream, β_1, depends on the sound speed for the matter on the stellar surface, which, in turn, depends on the gas temperature. A decrease/increase in β_1 indicates an increase/decrease in the matter outflow rate from the star, $\dot{M}$. In our case, the stream azimuth is constant within the uncertainties; the temperature of the star T_2 and the sizes and temperatures of the hot spot and hot line also did not change (within the uncertainties).

5.2. R Light Curves

Of the three R light curves (JD 294, 309, 316), only one (JD 309) was obtained during outburst (see Fig. 8). The total variation amplitude was 1.78^m, 2.08^m, and 1.62^m for JD 294, 309, and 316, respectively. However, the light-curve shape changed appreciably on JD 309, and the out-of-eclipse brightness increased by 0.6–0.7^m compared to the light curves on adjacent dates in the quiescent state. The RD temperature T_2 remained the same within the uncertainties at the beginning of the outburst and after its end. The WD temperature decreased slightly (by ∼8%) during the outburst and increased by ∼6% after the outburst, compared to the pre-outburst level. The parameters of the HL and HS remained unchanged within the uncertainties. Significant changes during outburst were observed only for the parameters of the disk. During quiescence, the disk radius remains at the level 0.5ξ and the half-thickness of its outer edge is ∼1.5°. During outburst, the disk radius increases

Table 3. Parameters of EX Dra obtained in the combined model from an analysis of the R and V light curves. The basic parameters $q = 1.34$, $i = 83.5°$, $R_1 = 0.0167a_0$, $\xi = 0.530$, and $\langle R_2 \rangle = 0.365a_0$ were fixed

Parameter	JD 281 (V)	JD 295 (V)	JD 294 (R)	JD 309 (R) outburst	JD 316 (R)
$\Delta m_{\max}$	−0.18	−0.13	−0.04	−0.79	−0.09
$\Delta m_{\min}$	1.96	2.01	1.67	1.32	1.53
T_1, K	20 500 ± 315	20 540 ± 210	20 310 ± 270	18 770 ± 125	22 610 ± 335
T_2, K	3640 ± 35	3625 ± 10	3600 ± 20	3640 ± 40	3660 ± 25
Accretion disk parameters					
e	0.001−0.04	0.001−0.04	0.001−0.01	0.001−0.02	0.002−0.02
R_d, ξ	0.40(2)	0.50(4)	0.51(1)	0.72(2)	0.49(4)
a, a_0	0.21(1)	0.26(2)	0.27(1)	0.38(1)	0.26(2)
$0.5\beta_d$,°	1.6(2)	0.9(1)	1.51(1)	0.42(3)	1.5(1)
T_{in}, K	22 360 ± 395	25 190 ± 305	20 930 ± 290	29 570 ± 485	23 180 ± 390
T_{out}, K	8065 ± 130	6350 ± 60	9330 ± 205	11800 ± 175	8415 ± 125
α_g	0.436(9)	0.577(5)	0.352(6)	0.325(8)	0.411(8)
α_e,°	46 ± 2	60 ± 33	56 ± 10	64 ± 30	46 ± 3
Hot line parameters					
a_v, a_0	0.016(5)	0.027(8)	0.03(1)	0.0013(7)	0.008(2)
b_v, a_0	0.22(2)	0.28(1)	0.29(1)	0.29(4)	0.25(2)
c_v, a_0	0.0062(3)	0.0051(6)	0.007(5)	0.004(1)	0.007(1)
$T_{ww,\max}$, K	34 560 ± 9550	41 540 ± 11 950	58 745 ± 16 440	63 035 ± 17 645	40 740 ± 16 650
$T_{lw,\max}$, K	29 560 ± 1220	34 385 ± 870	53 330 ± 2420	60 840 ± 13 250	36 415 ± 1940
β_1,°	17 ± 3	20 ± 2	9 ± 1	36 ± 2	21 ± 2
Hot spot radius					
R_{sp}, a_0	0.14(4)	0.16(2)	0.16(1)	0.13(5)	0.15(4)
Components' contribution to the combined flux from the system F_{full}					
Star	0.30(1)	0.34(2)	0.38(1)	0.22(1)	0.40(1)
White dwarf	0.13(2)	0.14(2)	0.06(1)	0.025(3)	0.08(1)
Disk with HS	0.49(6)	0.39(5)	0.54(5)	0.74(6)	0.46(4)
HL	0.08(2)	0.13(2)	0.02(1)	0.015(3)	0.06(1)
χ^2	1146	1475	1959	5518	2086

to ∼0.7ξ and the thickness of its edge decreases to ∼0.4°. Thus, the volume of the disk is, on average, larger by a factor of ∼1.2 in quiescence than during outburst; though the disk has a larger radius during outburst, it is thinner, has a higher density, and is hotter than before and after the outburst (T_{in} and T_{out} are higher than in quiescence and the disk temperature profile is less steep). The contributions from the system components to the total flux during quiescence coincide within the uncertainties; during the outburst, the period-averaged contribution from the disk reaches 0.74(6) of the total flux; i.e., it is a factor of 1.5 higher than in quiescence. The change in the stream azimuth β_1 testifies to a relatively high rate of mass outflow before the outburst, an abrupt decrease in this outflow during outburst, and a return to $\beta_1 \sim 20°$ after an outburst.

Table 4. Parameters of EX Dra obtained in the combined model from an analysis of the *Rc* light curves in quiescence, with the basic parameters fixed (see Table 3)

Parameter	JD 6819	JD 6960	JD 7106	JD 7118	JD 7123
N	138	809–10	1504–5	1562	1586
$m_{\max}$	13.93	14.09	14.11	14.20	14.29
$m_{\min}$	15.53	15.57	15.58	15.61	15.61
T_1, K	$19\,475 \pm 600$	$19\,615 \pm 210$	$20\,265 \pm 290$	$19\,475 \pm 275$	$20\,055 \pm 290$
T_2, K	3650 ± 22	3615 ± 17	3620 ± 17	3590 ± 12	3595 ± 20
Accretion disk parameters					
e	0.009(8)	0.010(9)	0.005(4)	0.03(2)	0.02(2)
R_d, ξ	0.32(1)	0.39(3)	0.54(6)	0.62(3)	0.43(2)
a, a_0	0.167(6)	0.21(2)	0.29(3)	0.32(2)	0.23(1)
$0.5\beta_d$, deg	1.7(4)	0.9(1)	1.1(2)	0.9(1)	0.6(1)
T_{in}, K	$20\,600 \pm 725$	$21\,055 \pm 280$	$20\,745 \pm 400$	$19\,565 \pm 100$	$23\,790 \pm 470$
T_{out}, K	$12\,975 \pm 425$	9890 ± 95	6730 ± 110	6355 ± 20	8210 ± 100
α_g	0.23(2)	0.427(8)	0.448(8)	0.435(6)	0.58(1)
α_e, deg	54 ± 40	60 ± 11	61 ± 45	45 ± 1	64 ± 2
Hot line parameters					
a_v, a_0	0.010(9)	0.040(4)	0.04(2)	0.05(3)	0.033(6)
b_v, a_0	0.16(4)	0.208(4)	0.31(2)	0.32(2)	0.236(6)
c_v, a_0	0.005(1)	0.004(1)	0.006(1)	0.006(1)	0.003(1)
$T_{ww,\max}$, K	$37\,920 \pm 30\,845$	$56\,090 \pm 13\,875$	$47\,690 \pm 10\,170$	$33\,205 \pm 12\,605$	$41\,740 \pm 12\,765$
$T_{lw,\max}$, K	$38\,095 \pm 7560$	$52\,445 \pm 1625$	$38\,175 \pm 2060$	$33\,195 \pm 3505$	$47\,245 \pm 4690$
β_1, deg	12 ± 2	12 ± 1	14 ± 1	12 ± 1	15 ± 1
Hot spot radius					
R_{sp}, a_0	0.12(5)	0.19(2)	0.14(2)	0.15(4)	0.17(2)
Components' contribution to the combined flux from the system F_{full}					
Star	0.400(7)	0.446(8)	0.476(8)	0.455(7)	0.523(2)
White dwarf	0.066(9)	0.088(9)	0.084(9)	0.090(9)	0.104(9)
Disk with HS	0.52(6)	0.40(3)	0.37(4)	0.40(3)	0.32(3)
HL	0.014(3)	0.066(9)	0.07(2)	0.055(9)	0.053(8)
χ^2	4030	1661	1961	5103	3393

Table 4. (Contd.)

Parameter	JD 7124	JD 7182	JD 7267	JD 7463	JD 7551
N	1590–1	1867	2271	3205–6	3624–5
$m_{\max}$	13.92	14.31	14.28	14.44	14.36
$m_{\min}$	15.60	15.59	15.60	15.69	15.67
T_1, K	$21\,240 \pm 240$	$19\,035 \pm 100$	$20\,385 \pm 310$	$18\,635 \pm 325$	$18\,560 \pm 295$
T_2, K	3615 ± 18	3605 ± 19	3605 ± 23	3560 ± 28	3565 ± 20
Accretion disk parameters					
e	0.02(1)	0.003(1)	0.03(2)	0.01(1)	0.03(2)
R_d, ξ	0.52(6)	0.351(1)	0.49(6)	0.42(2)	0.31(9)
a, a_0	0.27(3)	0.185(1)	0.25(3)	0.220(9)	0.161(5)
$0.5\beta_d$, deg	0.9(1)	0.5(1)	0.9(2)	0.8(1)	1.1(1)
T_{in}, K	$25\,735 \pm 330$	$19\,155 \pm 85$	$23\,220 \pm 390$	$18\,635 \pm 335$	$20\,695 \pm 480$
T_{out}, K	7775 ± 75	7380 ± 25	6515 ± 90	7105 ± 80	9480 ± 130
α_g	0.521(9)	0.449(1)	0.52(1)	0.50(1)	0.57(1)
α_e, deg	67 ± 45	40 ± 3	69 ± 2	47 ± 2	86 ± 2
Hot line parameters					
a_v, a_0	0.04(1)	0.022(1)	0.03(2)	0.030(6)	0.024(1)
b_v, a_0	0.32(1)	0.308(1)	0.30(2)	0.270(5)	0.147(8)
c_v, a_0	0.006(1)	0.002(1)	0.005(1)	0.003(1)	0.003(1)
$T_{ww,\max}$, K	$29\,145 \pm 3825$	$73\,425 \pm 6045$	$30\,895 \pm 7320$	$50\,520 \pm 10\,185$	$75\,620 \pm 31\,820$
$T_{lw,\max}$, K	$37\,060 \pm 3085$	$50\,635 \pm 2245$	$31\,830 \pm 4175$	$43\,040 \pm 1230$	$66\,480 \pm 2600$
β_1, deg	17 ± 2	9 ± 1	12 ± 2	9 ± 1	11 ± 1
Hot spot radius					
R_{sp}, a_0	0.14(2)	0.09(3)	0.10(4)	0.18(2)	0.17(2)
The components' light contribution to the combined flux from the system F_{full}					
Star	0.436(9)	0.518(9)	0.51(1)	0.526(8)	0.556(9)
White dwarf	0.088(8)	0.102(9)	0.11(1)	0.112(9)	0.108(9)
Disk with HS	0.39(3)	0.22(2)	0.33(3)	0.28(2)	0.29(3)
HL	0.086(9)	0.16(3)	0.05(1)	0.082(9)	0.046(7)
χ^2	1626	1176	1294	2233	2163

Table 5. Parameters of EX Dra obtained in the combined model from the analysis of the *Rc* light curves in outburst, with the basic parameters fixed (see Table 3)

Parameter	JD 6790	JD 6806	JD 6916	JD 7089	JD 7090	JD 7091	JD 7456	JD 7457
N	0	76	600	1424	1428–9	1433–4	3171	3176–77
$m_{\max}$	13.00	12.94	13.31	13.03	13.06	13.24	12.74	12.91
$m_{\min}$	15.09	15.37	15.41	15.29	15.33	15.44	15.21	15.31
T_1, K	20 690 ±	19 970 ±	21 490 ±	20 275 ±	20 255 ±	20 940 ±	18 890 ±	20 450 ±
	± 425	± 550	± 240	± 110	± 225	± 160	± 233	± 155
T_2, K	3624 ± 44	3650 ± 6	3640 ± 44	3610 ± 24	3645 ± 44	3650 ± 20	3650 ± 45	3605 ± 15
Accretion disk parameters								
e	0.003(3)	0.036(35)	0.017(27)	0.005(4)	0.005(15)	0.016(8)	0.01(2)	0.026(9)
R_d, ξ	0.72(3)	0.648(2)	0.67(2)	0.690(6)	0.659(14)	0.592(9)	0.678(10)	0.700(8)
a, a_0	0.38(2)	0.332(1)	0.349(9)	0.364(4)	0.348(8)	0.309(5)	0.357(5)	0.362(4)
$0.5\beta_d$, deg	0.6(1)	0.7(1)	1.6(2)	1.4(1)	0.7(1)	1.6(1)	1.0(1)	0.8(1)
T_{in}, K	24 195 ±	24 605 ±	29 710 ±	27 200 ±	24 785 ±	28 825 ±	31 780 ±	33 420 ±
	± 540	± 700	± 395	± 165	± 335	± 275	± 395	± 340
T_{out}, K	12 650 ±	12 400 ±	8815 ±	10 350 ±	12 515 ±	10 275 ±	11 585 ±	11 155 ±
	± 235	± 330	± 110	± 55	± 140	± 90	± 130	± 105
α_g	0.25(1)	0.24(1)	0.423(5)	0.335(3)	0.267(5)	0.375(4)	0.348(5)	0.374(3)
α_e, deg	74 ± 40	73 ± 15	60 ± 2	68 ± 35	81 ± 1	59 ± 1	61 ± 2	73 ± 2
Parameters of the hot line and the hot spot on the disk								
a_v, a_0	0.08(2)	0.043(26)	0.030(22)	0.079(12)	0.079(17)	0.052(24)	0.07(1)	0.049(13)
b_v, a_0	0.25(3)	0.36(1)	0.31(2)	0.259(7)	0.338(18)	0.278(11)	0.335(14)	0.25(2)
c_v, a_0	0.006(1)	0.007(2)	0.011(2)	0.013(1)	0.005(1)	0.010(1)	0.009(1)	0.007(1)
$T_{ww,\max}$, K	77 670 ±	86 470 ±	46 520 ±	33 650 ±	36 275 ±	48 535 ±	56 010 ±	108 475 ±
	± 35 700	± 35 170	± 22 220	± 16 690	± 13 700	± 21 145	± 19 465	± 38 540
$T_{lw,\max}$, K	59 360	58 965 ±	39 050 ±	30 660 ±	36 390 ±	39 730 ±	44 120 ±	78 880 ±
	± 2545	± 6895	± 2835	± 600	± 3125	± 1385	± 1760	± 2560
β_1, deg	30 ± 6	18 ± 7	17 ± 3	24 ± 2	20 ± 1	17 ± 2	22 ± 3	27 ± 2
R_{sp}, a_0	0.13(5)	0.12(9)	0.13(3)	0.21(2)	0.19(3)	0.16(3)	0.20(3)	0.17(3)
Components' contribution to the combined flux from the system F_{full}								
Star	0.176(4)	0.188(6)	0.277(1)	0.198(7)	0.199(5)	0.267(9)	0.196(9)	0.224(15)
WD	0.033(3)	0.032(4)	0.045(5)	0.030(4)	0.034(3)	0.039(5)	0.022(3)	0.030(3)
Disk with HS	0.77(5)	0.72(6)	0.66(5)	0.75(6)	0.73(5)	0.66(5)	0.73(5)	0.73(5)
HL	0.019(3)	0.06(1)	0.018(3)	0.022(5)	0.037(6)	0.034(7)	0.052(8)	0.016(3)
χ^2	5565	3478	2662	508	1750	1214	3121	1716

Table 6. Parameters of EX Dra obtained in the model with spots on the secondary from an analysis of *Rc* light curves during outburst, with the basic parameters fixed (see Table 3)

Parameter	JD 6805	JD 6834	JD 7108	JD 7167	JD 7268	JD 7271
N	71	209	1514	1795	2276	2290−1
$m_{\max}$	13.43	14.13	14.30	14.19	14.44	14.55
$m_{\min}$	15.52	15.53	15.61	15.59	15.64	15.64
T_1, K	$21\,655 \pm 205$	$21\,660 \pm 5$	$21\,245 \pm 280$	$20\,550 \pm 330$	$20\,215 \pm 190$	$19\,345 \pm 145$
T_2, K	3645 ± 27	3650 ± 40	3605 ± 13	3610 ± 25	3590 ± 18	3595 ± 10
Accretion disk parameters						
e	0.034(7)	0.08(2)	0.13(2)	0.06(3)	0.016(2)	0.019(3)
R_d, ξ	0.57(2)	0.69(1)	0.42(3)	0.49(5)	0.43(4)	0.34(1)
a, a_0	0.291(12)	0.337(7)	0.199(12)	0.243(22)	0.225(23)	0.175(5)
$0.5\beta_d$, deg	1.2(1)	0.74(1)	0.85(8)	1.1(1)	0.9(1)	0.7(1)
T_{in}, K	$32\,750 \pm 330$	$26\,440 \pm 100$	$23\,715 \pm 430$	$21\,520 \pm 445$	$21\,510 \pm 280$	$20\,060 \pm 220$
T_{out}, K	9375 ± 80	6935 ± 20	7610 ± 110	7235 ± 125	6170 ± 75	7735 ± 80
α_g	0.479(6)	0.546(1)	0.545(12)	0.460(9)	0.501(8)	0.417(6)
α_e, deg	59 ± 2	104 ± 1	71 ± 2	57 ± 1	65 ± 5	62 ± 21
Parameters of the hot line (HL) and the hot spot on the disk						
a_v, a_0	0.055(2)	0.037(1)	0.019(3)	0.035(8)	0.020(9)	0.016(4)
b_v, a_0	0.263(9)	0.247(1)	0.263(11)	0.296(9)	0.294(8)	0.269(8)
c_v, a_0	0.008(1)	0.006(1)	0.004(1)	0.006(1)	0.004(1)	0.003(1)
$T_{ww,\max}$, K	$73\,115 \pm 18\,140$	$101\,900 \pm 80$	$34\,520 \pm 4600$	$48\,255 \pm 9400$	$37\,290 \pm 4550$	$37\,385 \pm 3545$
$T_{lw,\max}$, K	$54\,975 \pm 1565$	$79\,475 \pm 60$	$38\,475 \pm 3700$	$38\,035 \pm 1345$	$28\,345 \pm 1080$	$28\,510 \pm 1750$
β_1, deg	20 ± 1	26 ± 1	11 ± 1	11 ± 2	12 ± 2	11 ± 2
R_{sp}, a_0	0.19(2)	0.11(2)	0.11(2)	0.12(3)	0.08(2)	0.04(2)
Parameters of hot spots on the secondary						
R_{s1}, $R_2(i)$	0.39(6)	0.40(6)	0.19(7)	0.49(7)	0.34(5)	0.39(4)
f_{s1}	0.93(3)	0.87(9)	0.93(5)	0.94(3)	0.90(7)	0.96(1)
η_{s1}, deg	29 ± 3	73 ± 31	20 ± 14	35 ± 10	49 ± 11	38 ± 6
ϕ_{s1}, deg	34 ± 20	23 ± 21	24 ± 22	22 ± 14	22 ± 13	44 ± 15
R_{s2}, $R_2(i)$	0.26(9)	0.60(9)	0.23(8)	0.31(2)	0.31(9)	0.49(1)
f_{s2}	0.8(2)	0.33(5)	0.91(8)	0.99(1)	0.85(9)	0.90(6)
η_{s2}, deg	43 ± 7	85 ± 6	97 ± 23	21 ± 20	99 ± 6	92 ± 2
ϕ_{s2}, deg	102 ± 16	208 ± 11	149 ± 59	121 ± 30	128 ± 15	154 ± 3
Components' contribution to the combined flux from the system F_{full}						
Star	0.32(2)	0.43(1)	0.51(2)	0.45(1)	0.50(1)	0.50(1)
WD	0.056(5)	0.10(1)	0.12(1)	0.10(1)	0.12(1)	0.12(1)
Disk with HS	0.59(4)	0.46(3)	0.29(2)	0.38(3)	0.32(2)	0.32(3)
HL	0.034(5)	0.015(3)	0.08(2)	0.07(2)	0.06(1)	0.06(1)
χ^2	2151	6867	1704	1682	853	464

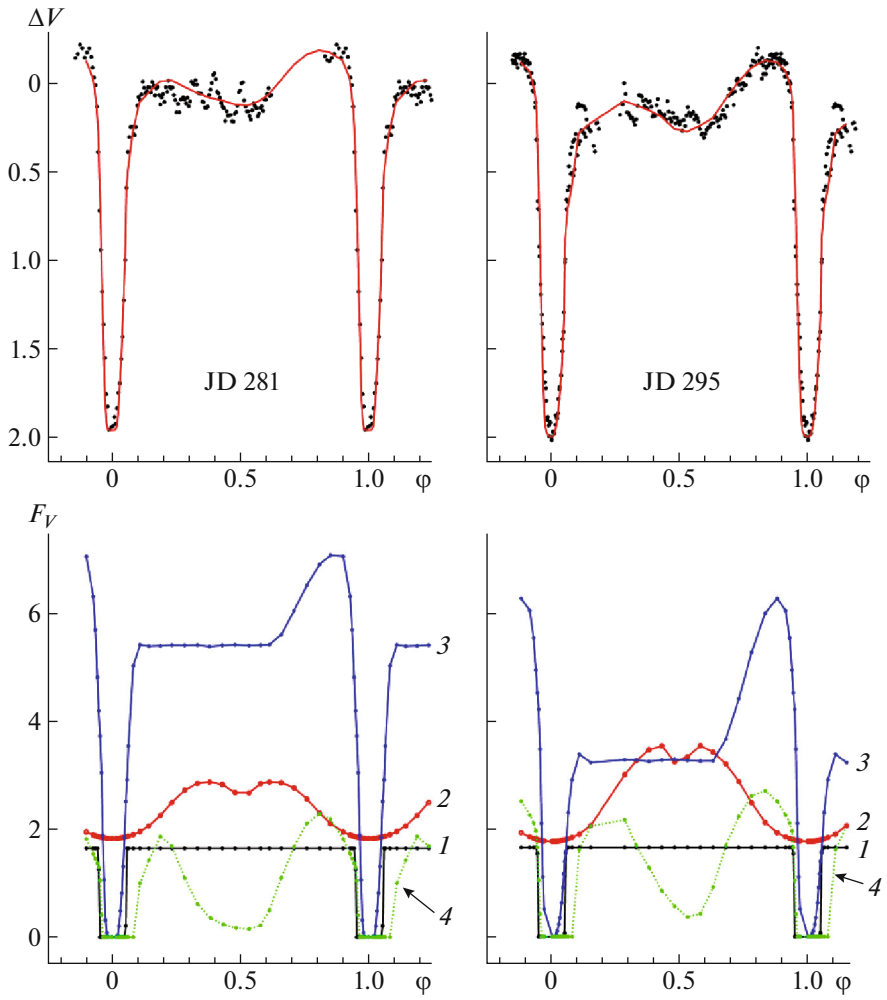

Fig. 7. V observations of EX Dra obtained in 2010 at the Ondrejov Observatory. The dots in the upper panels show the unaveraged light curves and the solid curves show the theoretical light curves synthesized with the parameters from Table 3. The lower panels display the contributions of the light from the WD (1), the RD secondary (2), the accretion disk with the hot spot (3), and the hot line (4) to the total flux (in relative units).

5.3. Rc Light Curves

Our data in the Rc band are more numerous; however, in contrast to the V and R data, they are unevenly distributed in the $N \sim 0-3625$ interval, where N is the number of the orbital cycle relative to the first minimum observed in this filter ($N = 0$ for JD 6790.48864, see Table 2). We cannot follow continuous variations of the system parameters, but can isolate several interesting groups.

1. The light curves for JD 6805 ($N = 71$, Table 6), JD 6806 ($N = 76$, Table 5), and JD 6819 ($N = 138$, Table 4). The light curve for JD 6806 was obtained during outburst, the those for JD 6805 and 6819 during quiescence. Before the outburst (JD 6805), cool spots are inferred on the surface of the RD, near the tip of the "nose" of the star, with radii of 0.3–0.4 of the RD's radius in the region considered (see Fig. 14). Their contrast is not large (~0.8–0.9), but the spot magnetic fields and the general decrease of the temperature in their region lead to a decrease in the matter outflow rate.

Comparing the system parameters, we find that the disk radius is smaller just before the outburst than on later dates ($R_d/\xi \sim 0.57$, 0.65, and 0.32 for JD 6805, 6806, and 6819, respectively), while the thickness of its outer edge is larger than during the outburst ($0.5\beta_d \sim 1.2°$, 0.7°, and 1.7°, respectively); the apparent radius of the disk decreases almost twofold after the outburst, with a corresponding increase in the thickness of the outer edge. The radial temperature distribution in the disk is closer to the equilibrium distribution before than during and after the outburst ($\alpha_g \sim 0.48$, 0.24, and 0.23, respectively), but the α_g values in outburst and quiescence are generally comparable. The temperature

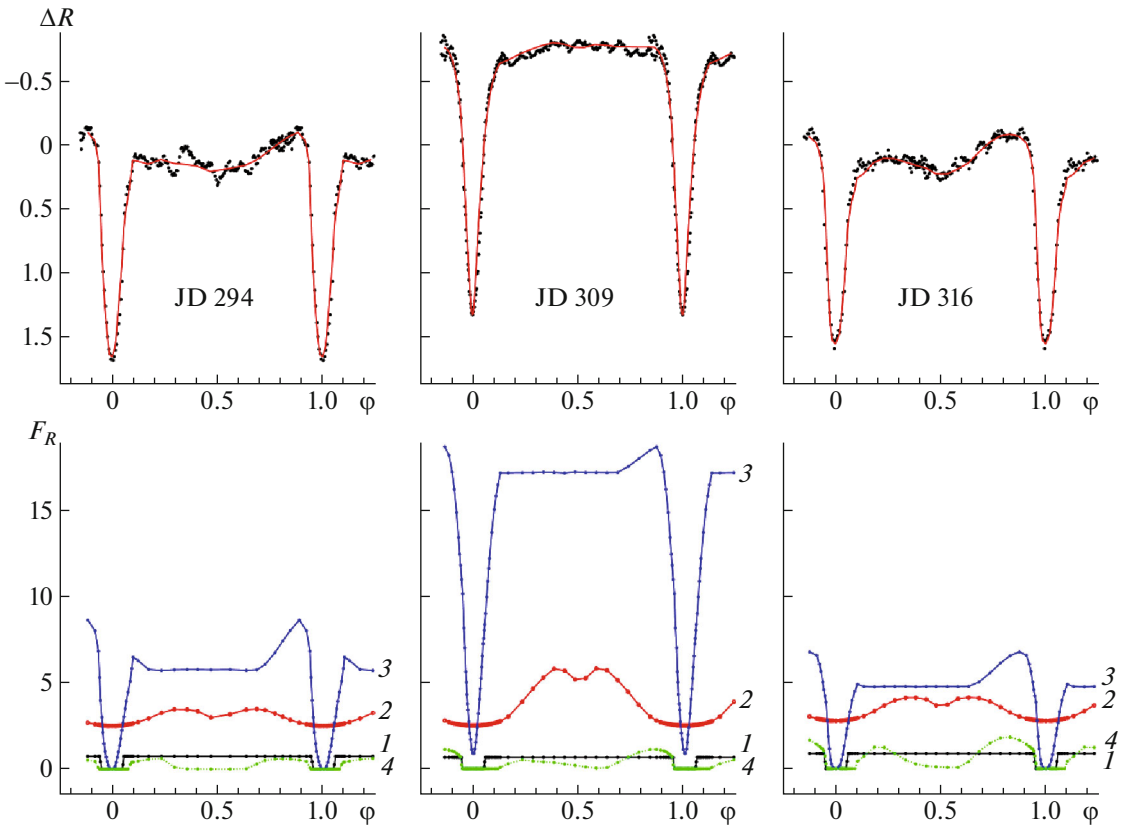

Fig. 8. *R* observations of EX Dra obtained in 2010 at the Ondrejov Observatory. The notation is the same as in Fig. 7.

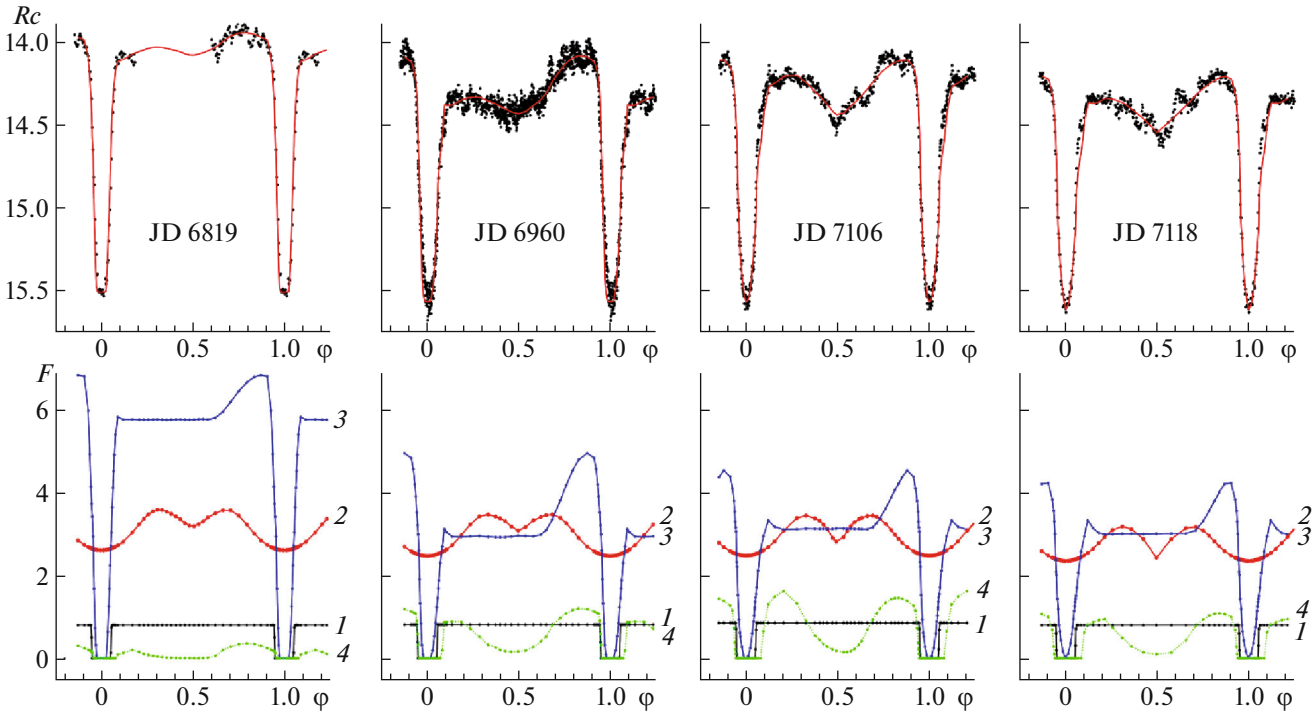

Fig. 9. *Rc* observations of EX Dra obtained in 2014–2015 at the Sternberg Astronomical Institute Crimean Astronomical Station during quiescence. The notation is the same as in Fig. 7.

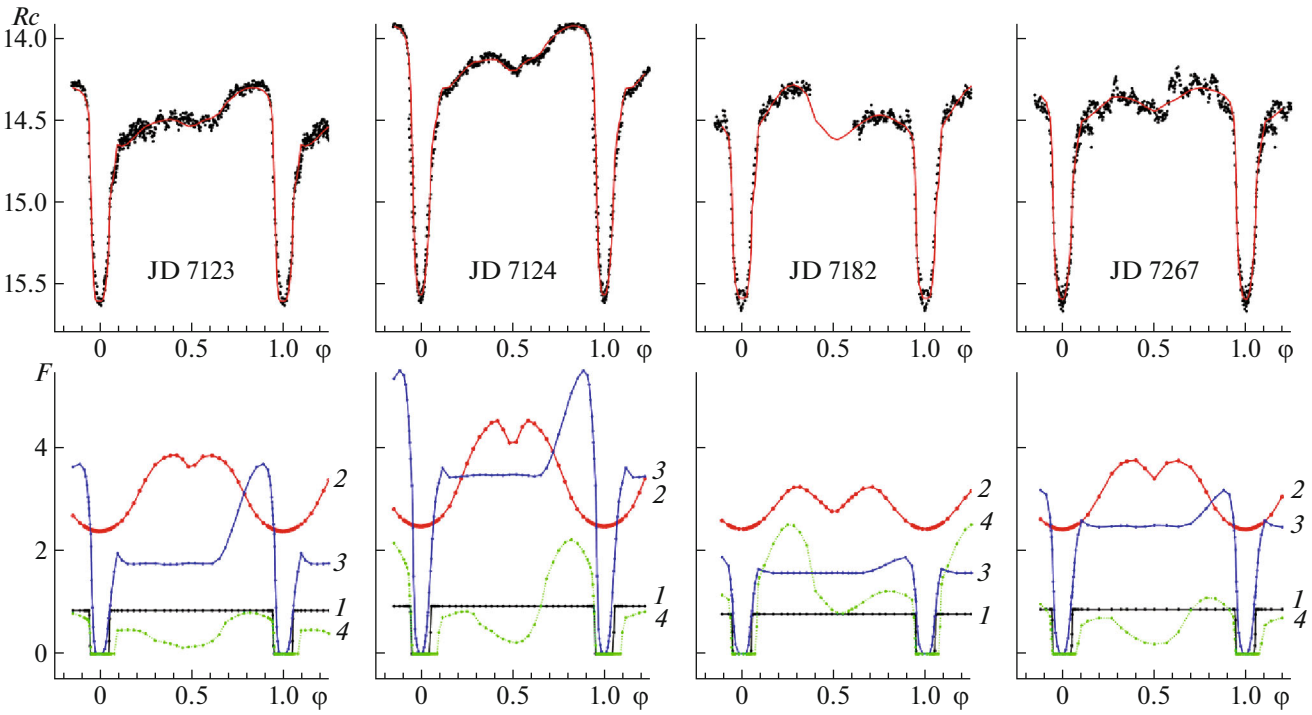

Fig. 10. Same as Fig. 9 for observations of EX Dra in 2015.

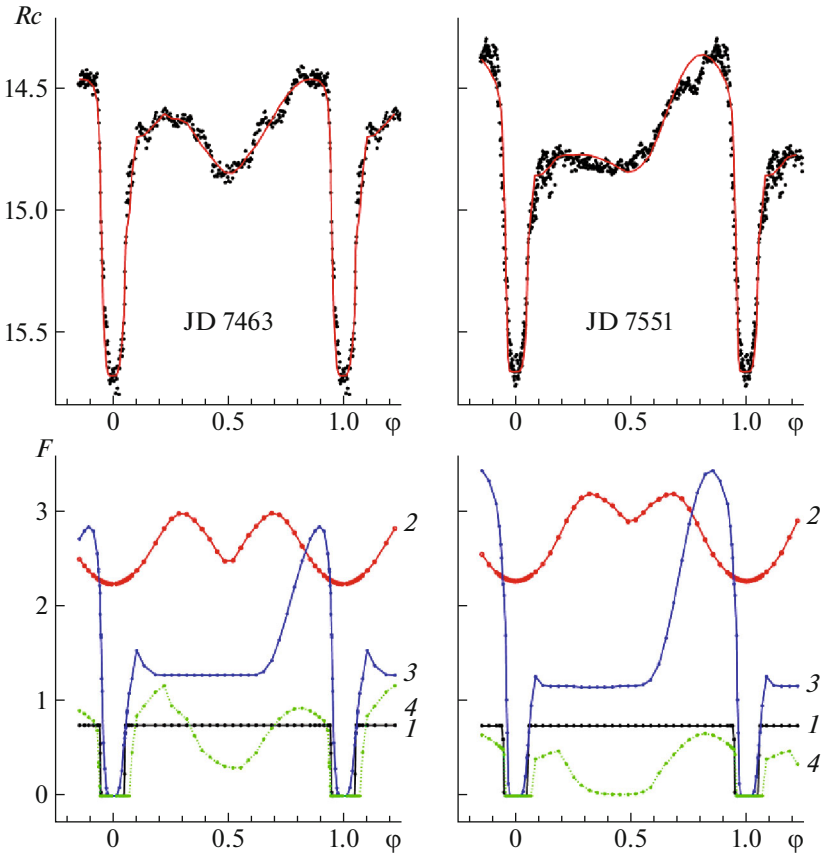

Fig. 11. Same as Fig. 9 for observations of EX Dra in 2016.

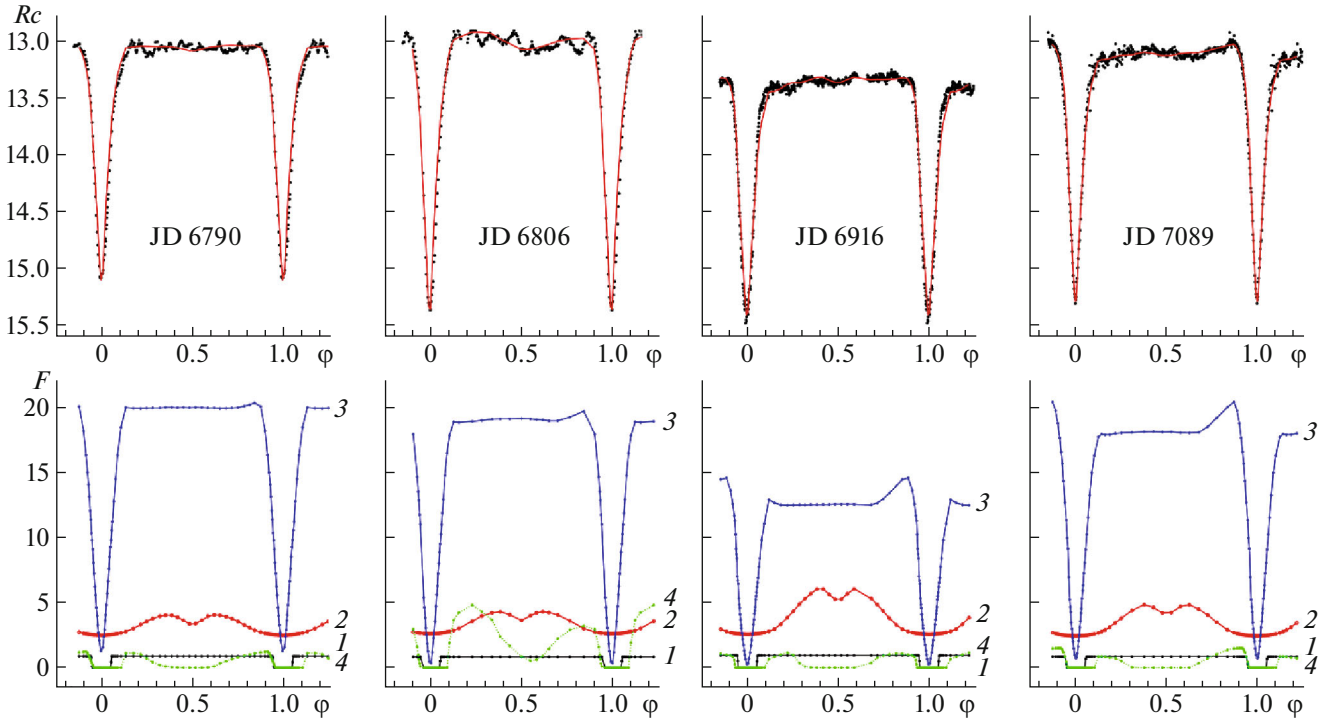

Fig. 12. *Rc* observations of EX Dra obtained at the Sternberg Astronomical Institute's Crimean Astronomical Station in 2014–2015 during outburst. The notation is the same as in Fig. 7.

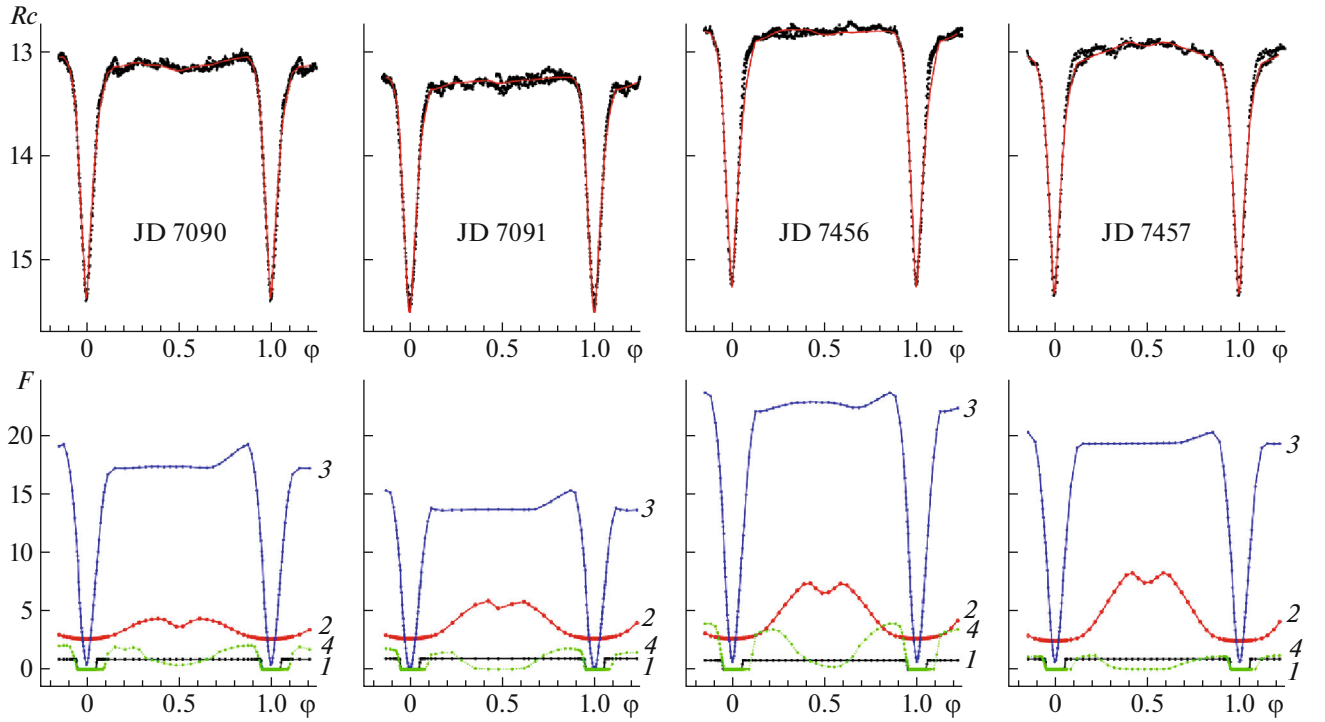

Fig. 13. Same as Fig. 12 for observations of EX Dra on March 8–9, 2015 and March 8–9, 2016.

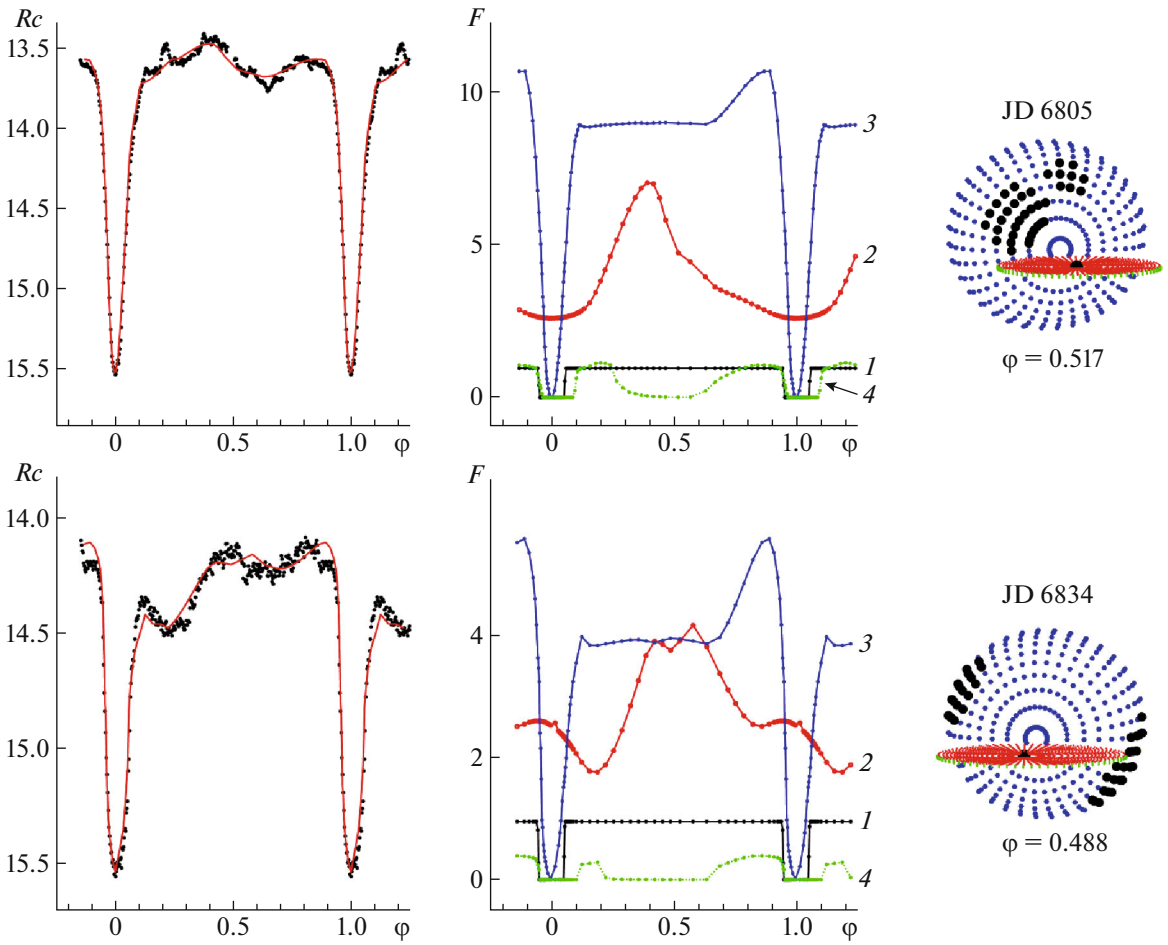

Fig. 14. *Rc* light curves of EX Dra obtained in 2014 (in quiescence). The left panels show unaveraged data points and theoretical light curves synthesized in the spot model with the parameters from Table 6. The middle panels show the contributions to the combined flux of the system (in relative units) from the WD (1), RD (2), accretion disk with the hot spot (3), and hot line (4). The right panels show schematic images of the system for the orbital phases shown.

variations at the outer edge of the disk are small ($T_{\rm out} \sim 9400-13\,000$ K); the temperature reaches $T_{\rm in} \sim 33\,000$ K in the boundary layer before outburst, while it decreases during and after the outburst ($T_{\rm in} \sim$ 25 000 and 20 500 K).

2. The light curves on JD 7089 ($N = 1424$), JD 7090 ($N = 1428-9$), JD 7091 ($N = 1433-4$). All three light curves were obtained during outburst (Table 5); the highest flux was observed on the first date. The outburst durations were at least $10P_{\rm orb}$. The parameters varied as follows for JD 7089, 7090, 7091, respectively: $T_2 = 3610$, 3645, 3650 K; $\beta_1 =$ 24°, 20°, 17°; $R_s/\xi = 0.69$, 0.66, 0.59; $0.5\beta_d =$ 1.4°, 0.7°, 1.6°; $\alpha_g = 0.34$, 0.27, 0.38; $T_{\rm in} = 27\,000$, 25 000, 29 000 K; $T_{\rm out} = 10\,300$, 12 500, 10 300 K; $F_d/F_{\rm full} = 0.75$, 0.73, 0.66; $T_{lw,\max}/1000 = 30-31$, 33–39, 38–41; $R_{sp}/a_0 = 0.21$, 0.19, 0.16.

3. The light curves during outburst (Table 5) on JD 7456 ($N = 3171$), JD 7457 ($N = 3176-7$), and in quiescence on JD 7463 ($N = 3205-6$, Table 4). The disk parameters during the outburst are close to those obtained for Group 2, and its contribution to the total flux at maximum remains about 73%, with $\alpha_g \sim$ 0.35–0.37. In the transition to quiescence, the disk radius decreases to 0.42ξ, as for Group 1; the disk temperature in the boundary layer and outer edge decreases, and the temperature distribution approaches the equilibrium distribution.

4. The quiescence light curves on JD 7106 ($N =$ 1504–5, Table 4), JD 7108 ($N = 1514$, Table 6), JD 7118 ($N = 1562$, Table 4), JD 7123 ($N = 1586$, Table 4), JD 7124 ($N = 1590-91$, Table 4). For one of these light curves (JD 7108), the displacement of the secondary minimum to phase $\varphi \sim 0.6$ suggests the presence of spots on the surface of the secondary, with one of the spots also situated near the tip of the star's "nose", distorting the ellipsoidal shape of the secondary's contribution. We were able to adequately

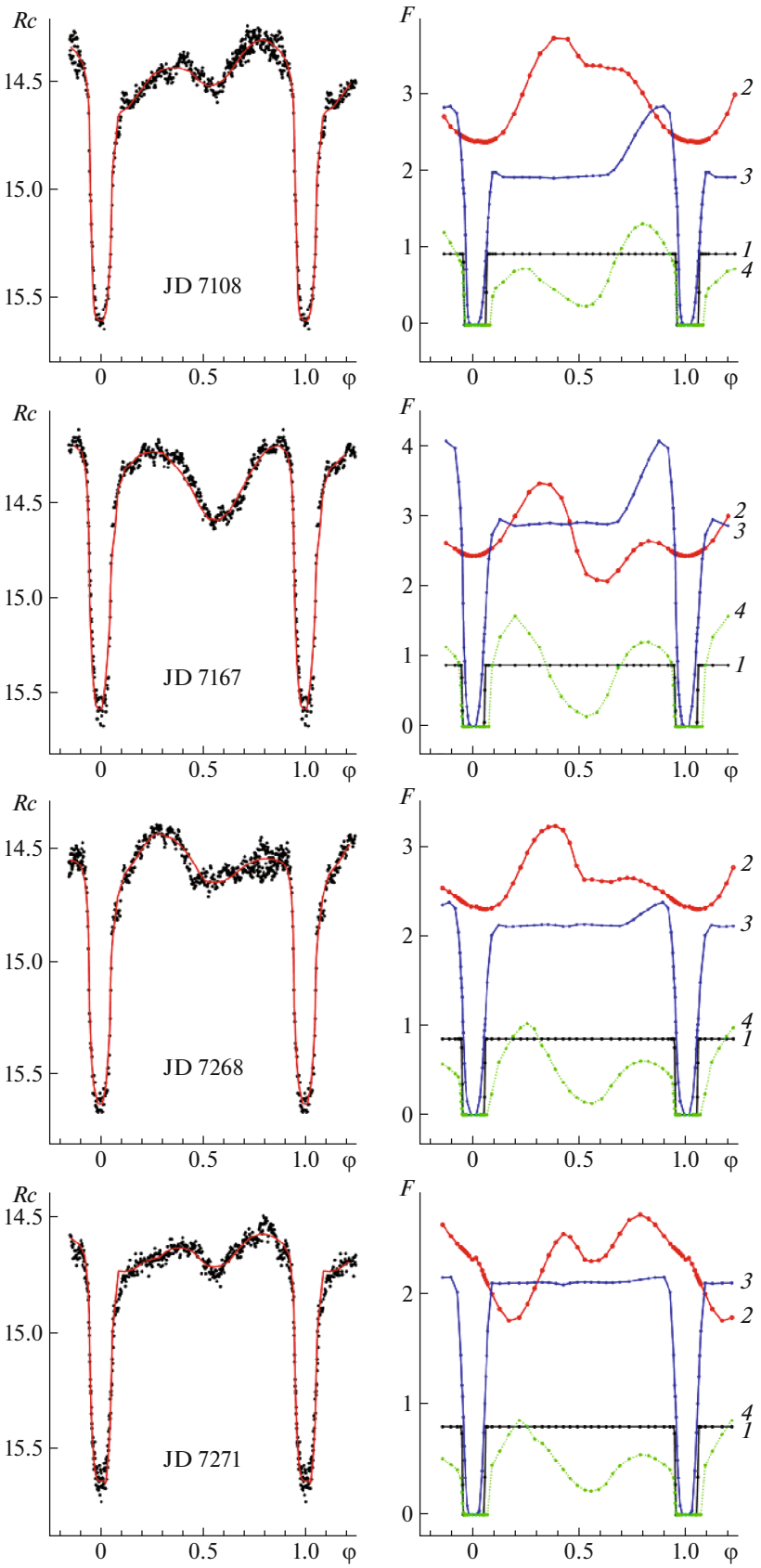

Fig. 15. *Rc* observations of EX Dra obtained in 2015 during quiescence. The left panels show unaveraged data points and theoretical light curves synthesized in the spot model with the parameters from Table 6. The right panels show the contributions from the system components to the total flux in relative units. The notation is the same as in Fig. 14.

fit the other light curves in the model without spots. The last of these light curves (JD 7124) features an appreciable increase in the radiation flux, from the disk and also the HS and HL. If we are observing the pre-outburst state of the system in this group of light curves, this is accompanied by the appearance of spots on the secondary, in the region of the tip of the star's "nose". Here, we observe a relatively high matter outflow rate ($\beta_1 \sim 11°-12°$). After a time interval of about $(20-30)P_{\rm orb}$, the matter outflow rate decreases ($\beta_1 \sim 15°-17°$), and the disk radius first decreases (JD 7123, $R_d/\xi \sim 0.43$), then increases (JD 7124, $R_d/\xi \sim 0.52$); the radiation from the HS simultaneously increases.

6. DISCUSSION

In a series of papers, Baptista [14] and Baptista et al. [25–27] consider two models for dwarf-nova outbursts. According to the MTIM model [28], an outburst is a time-dependent response of a viscous accretion disk to an increase of the mass-transfer rate from the donor star. In the DIM model [29], matter is transferred at a nearly constant rate to a disk with low viscosity α_0[7] and is accumulated until a critical surface density is reached at a given radius. A hot wave arises, resulting in the disk switching to a high-viscosity mode ($\alpha \sim 0.1\alpha_0$), enabling the gas to quickly propagate inward and be accreted onto the WD.

The MTIM model predicts small variations of α in the transition from quiescence to the active state (outburst); the bright, stationary disk reacts to changes in the mass-outflow rate $\dot{M}$ in the same way as during the same short time interval during outburst. Due to the abrupt increase in $\dot{M}$, this model predicts an overflow of the gaseous stream and an increase in the emission along its trajectory outside the accretion disk at the beginning of an outburst. The disk responds to this unexpected addition of matter with low specific angular momentum by decreasing its size; it then expands due to the redistribution of angular momentum. The quiescent viscosity of the disk is approximately the same as in outburst, $\alpha \sim 0.2-0.7$ for different systems. Objects for which this outburst model appears valid are called DDNs systems.

In the DIM model, reproducing the observed outburst durations and amplitudes requires the disk viscosity to be an order of magnitude lower in quiescence than in outburst. This model predicts a nonstationary disk that is not bright in quiescence and responds weakly to variations of $\dot{M}$. There is not a stronger gaseous stream or contraction of the disk prior to outburst: the disk simply expands to its maximum possible size. The outflowing matter accumulates in an unstable, low-viscosity disk. The radial temperature distribution in outburst is close to the relation $T \sim R^{-3/4}$ ($\alpha_g \sim 0.75$) expected for an optially thick, steady-state disk [31], while this distribution in quiescence is fairly flat, $\alpha_g \ll 0.75$, with $T_d < 6000$ K everywhere [32]. Thus, the viscosity of the accretion disk is much lower than during outburst, and the disk is far from the steady state. Objects for which this outburst model appears valid are called MDNs systems.

Thus, analysis of the observational data suggests the presence of two different groups of dwarf novae. While the DIM model can explain the outbursts of one of these groups, outbursts of dwarf novae in the other group can be explained only using the MTIM model. The question is not which of the models is valid and which is not, but instead which mechanism should be applied for a particular system.

Membership in a particular group is also indicated by the morphology of the light curve of an eclipsing system: since the DIM model assumes that weak accretion onto the WD, the quiescent light curves are dominated by the contribution from the HS (a strong orbital hump), and a two-stage eclipse is observed. On the other hand, an MTIM viscous quiescent disk suppresses radiation from the HS, the orbital hump in the light curve is weak or completely absent, and smooth eclipse profiles without steps similar to those in nova-like systems are observed.

Comparing eclipse maps during the brightness increase at the beginning of an outburst and in quiescence suggests that the outbursts in the EX Dra system correspond to episodes of enhanced matter outflow from the secondary [7, 14], as predicted by the MTIM model. The analysis of our observations of the cataclysmic variable EX Dra testifies that this system is a DDNs object. This is due to the high viscosity of the matter in the accretion disk, small changes in the viscosity in the transition from quiescence to the active state, and the contraction of the accretion disk and increase of the radiation from the HS and HL prior to outburst.

7. CONCLUSIONS

We have analyzed long-term photometric observations of the dwarf nova EX Dra, a system with a

[7] Here, $\alpha_0 \simeq \frac{v_h}{c_s} = 0.082 \left[\frac{v_f}{\rm km/s}\right] \left(\frac{T_f}{18\,000\ {\rm K}}\right)^{-1/2}$ [30]; v_f is the velocity of the shock front traversing the accretion disk, c_s the sound speed in this front, and T_f the temperature of the matter in the shock.

long orbital period, in quiescence, the pre-outburst state, and the active state. Our observations were obtained at the Crimean Astronomical Station of the Sternberg Ansronomical Institute (2014–2016) and the Ondrejov Observatory of the Astronomical Institute of Czech Academy of Sciences (2010), in the *Rc*, *V*, *R* filters. Our analysis of these observations leads to the following conclusions.

1. The binary's orbital period derived from our observations confirms the value found earlier [4].

2. A combined model without spots on the RD surface and taking into account the presence of a hot spot on the lateral surface of the accretion disk and the contribution of light from the stream near the outer edge of the disk can successfully be applied to determine the parameters of EX Dra in different states of the system's activity for 80% of the studied light curves.

3. The remaining six observed light curves (20%) could not be satisfactorily fit with theoretical ones produced using this model. Accordingly, we added one or two dark spots on the surface of the RD secondary to the combined model. Taking the existence of these spots into account, we were able to qualitatively reproduce the existence of secondary minima at phases differing from $\varphi \sim 0.5$.

4. A detailed study of the behavior of the system parameters we have derived and their changes in the transition from quiescence to the active state confirms that EX Dra is a DDNs system whose outbursts are produced by the MTIM model; i.e., the outbursts in this dwarf-nova system are due to enhanced matter outflow from the secondary.

5. At this stage in our studies, we cannot rule out the possible influence of spot activity on the surface of the late-type secondary on variations of the matter outflow rate from the star. New observations of this system are needed to test this hypothesis.

FUNDING

This work was supported by the Russian Foundation for Basic Research (grant no. 17-52-53200), and also by a grant from the Development Program of the Moscow State University for the Leading Scientific School "Physics of Stars, Relativistic Objects, and Galaxies."

ACKNOWLEDGMENTS

The authors thank K. Hornoch, J. Vrastil, and H. Kucáková for assistance during the observations at the Ondrejov Observatory and V.P. Goranskij for the possibility of using his period-determination software.

REFERENCES

1. B. Warner, *Cataclysmic Variable Stars*, Vol. 28 of *Cambridge Astrophysics Series* (Cambridge Univ. Press, Cambridge, 1995).
2. N. Bade, H.-J. Hagen, and D. Reimers, in *Proceedings of the 23rd ESLAB Symposium,* Ed. by J. Hunt and B. Battrick, ESA SP-296 (ESA, Noordwijk, 1989), p. 883.
3. H. Barwig, H. Fiedler, D. Reimers, and N. Bade, in *IAU Symposium 165: Compact Stars in Binary Systems,* Ed. by H. van Woerden (Kluwer, Dordrecht, 1993), p. 89.
4. L. Pilarčik, M. Wolf, P. A. Dubovský, K. Hornoch, and L. Kotková, Astron. Astrophys. **539**, A153 (2012).
5. I. Billington, T. R. Marsh, and V. S. Dhillon, Mon. Not. R. Astron. Soc. **278**, 673 (1996).
6. H. Fiedler, H. Barwig, and K. H. Mantel, Astron. Astrophys. **327**, 173 (1997).
7. R. Baptista, M. S. Catal'an, and L. Costa, Mon. Not. R. Astron. Soc. **316**, 529 (2000).
8. A. W. Shafter and J. N. Holland, Publ. Astron. Soc. Pacif. **115**, 1105 (2003).
9. N. I. Shakura and R. A. Sunyaev, Astron. Astrophys. **24**, 337 (1973).
10. A. V. Halevin and A. A. Henden, Inform. Bull. Var. Stars, No. 5833 (2008).
11. V. Joergens, H. C. Spruit, and R. G. M. Rutten, Astron. Astrophys. **356**, L33 (2000).
12. D. A. Smith and V. S. Dhillon, Mon. Not. R. Astron. Soc. **301**, 767 (1998).
13. C. Knigge, Mon. Not. R. Astron. Soc. **373**, 484 (2006).
14. R. Baptista, Mem. Soc. Astron. Ital. **83**, 530 (2012).
15. C. Hellier, J. Kemp, T. Naylor, F. M. Bateson, A. Jones, D. Overbeek, R. Stubbings, and K. Mukai, Mon. Not. R. Astron. Soc. **313**, 703 (2000).
16. T. S. Khruzina, I. B. Voloshina, and V. G. Metlov, Astron. Rep. **60**, 971 (2016).
17. T. S. Khruzina, I. B. Voloshina, S. Qian, and V. G. Metlov, Astron. Rep. **62**, 31 (2018).
18. T. S. Khruzina, Astron. Rep. **55**, 425 (2011).
19. T. S. Khruzina and A. M. Cherepashchuk, Sov. Astron. **39**, 178 (1985).
20. A. M. Cherepashchuk, N. A. Katysheva, T. S. Khruzina, S. Yu. Shugarov, A. M. Tatarnikov, M. A. Burlak, and N. I. Shatsky, Monthly Not. Roy. Astron. Soc. **483**, 1067 (2019).
21. L. B. Lucy, Zeitschr. Astrophys. **65**, 89 (1967).
22. D. Himmelblau, *Applied Nonlinear Programming* (McGraw-Hill, New York, 1972), p. 163.

23. T. S. Khruzina, A. M. Cherepashchuk, D. V. Bisikalo, A. A. Boyarchuk, and O. A. Kuznetsov, Astron. Rep. **47**, 214 (2003).
24. G. M. H. J. Habets and J. R. W. Heintze, Astron. Astrophys. Suppl. Ser. **46**, 193 (1981).
25. R. Baptista and M. S. Catalán, Astrophys. J. **539**, L55 (2000).
26. R. Baptista and A. Bortoletto, Astron. J. **128**, 411 (2004).
27. R. Baptista, R. F. Santos, M. Faúndez-Abans, and A. Bortoletto, Astron. J. **134**, 867 (2007).
28. G. T. Bath, Mon. Not. R. Astron. Soc. **171**, 311 (1975).
29. J. P. Lasota, New Astron. Rev. **45**, 449 (2001).
30. J. K. Cannizzo, in *Accretion Disks in Compact Stellar Systems,* Ed. by J. C. Wheeler (World Scientific, Singapore, 1993), p. 6.
31. K. Horne and M. C. Cook, Mon. Not. R. Astron. Soc. **214**, 307 (1985).
32. J. Wood, K. Horne, G. Berriman, R. Wade, D. O'Donoghue, and B. Warner, Mon. Not. R. Astron. Soc. **219**, 629 (1986).

Translated by N. Samus'